Summary of Professional Accomplishments

Olaf Morawski

Table of content

1. Name

Olaf Morawski

2. Diplomas, degrees conferred in specific areas of science

1983 – Master of Science in Physics, Faculty of Physics, University of Warsaw
1991 – PhD in Physics, Institute of Physics Polish Academy of Science, Warsaw
„Electronic states and photophysical processes in chemically mixed crystals of acridine”

3. Information on employment in research institutes or faculties/departments

1985-1993 – employment in *Institute of Physics Polish Academy of Science*, Warsaw
1993-1995 –post-doc scholarship in *Max-Planck-Institut für biophysikalische Chemie*, Goettingen, Germany
1996-2012 – work outside science in IT departments in charge of data analysis (*P&G*, *Sequent*, *HP*, *CDM*)
2013 - – employment in *Institute of Physics Polish Academy of Science*, Warsaw

4. Description of the achievements, set out in art. 219 § 1 point 2 of the Act

4.1 Scientific achievement (habilitation achievement)

4.1.1 Title of the scientific achievement

Experimental proof of concept for photocatalytic cleavage of methanol and water via the radical pathway and photochemical hydrogen storage.

4.1.2 Abstract

In a series of five papers, it was experimentally demonstrated that water and alcohols can be photocatalytically cleaved into two radicals: an atomic hydrogen and a residue (hydroxy for water, methoxy for methanol, etc.) thus confirming a new concept, previously only theoretically considered, for obtaining hydrogen from protic liquids. This process allows the photochemical storage of hydrogen via the radical pathway, without generating ions as in electrolysis or the commonly studied photo-electrochemical approach. In the course of this work, the conditions necessary for the photocatalytic process were determined and the chromophores capable of hydrogen accumulation were identified. Side processes occurring during the generation of highly reactive radicals in the liquid and their impact on hydrogenated chromophore molecules are also discussed.

4.1.3 Publications on which the scientific achievement is based

[P1] O. Morawski, K. Izdebska, E. Karpiuk, J. Nowacki, A. Suchocki and A. L. Sobolewski
Phys. Chem. Chem. Phys., **2014**, 16, 15256–15262
Photoinduced water splitting with oxotitanium tetraphenylporphyrin

[P2] Olaf Morawski, Katarzyna Izdebska, Elena Karpiuk, Andrzej Suchocki, Yaroslav Zhydachevskyy and Andrzej L. Sobolewski
J. Phys. Chem. C, **2015**, 119, 14085–14093

Titanyl Phthalocyanine as a Water Photooxidation Agent

[P3] Olaf Morawski, Jerzy Karpiuk, Paweł Gawryś and Andrzej L. Sobolewski
Phys. Chem. Chem. Phys., **2020**, 22, 15437−15447
Aggregation controlled photoluminescence of hexaazatri-naphthylene (HATN) – an experimental and theoretical study

[P4] Olaf Morawski, Paweł Gawryś, Jarosław Sadło and Andrzej L. Sobolewski
ChemPhysChem, **2022**, 23, e202200077
Photochemical Hydrogen Storage with Hexaazatrinaphthylene

[P5] Olaf Morawski, Paweł Gawryś and Andrzej L. Sobolewski
J. Phys. Chem. A, **2023**, 127, 8871–8881
Harnessing Proton Coupled Electron Transfer for Hydrogenation of Aza-Arenes: Photochemistry of Quinoxaline Derivatives in Methanol

4.1.4 Description of the scientific achievement

Description of the scientific achievement is presented in section 4.1.4.3 of this chapter and is preceded by an introduction illustrating the broader background of the research (4.1.4.1) as well as a discussion of the novel idea of hydrogen extraction via the radical pathway from protic solvents (4.1.4.2)

4.1.4.1 Introduction - broad research background

Increasing global warming and the threats associated with it are associated with the emission of greenhouse gases, mainly water vapor, CO_2, methane and nitrogen oxides [1]. It is believed that 70% of CO_2, CH_4 and N_2O emissions have anthropogenic sources [2]. Limiting these emissions or reducing them significantly may give hope for a return to a state of balance in which nature automatically eliminates greenhouse gases generated in natural biological processes. Hence the concept of a zero-emission economy that does not produce additional amounts of greenhouse gases. Hydrogen is mainly indicated as the fuel for a zero-emission economy [3], although methanol and other alcohols are also mentioned [4]. Fuel cells generating electricity from the fuel oxidation reaction have been developed for both energy carriers, with a number of device variants created for hydrogen and the $H_2 + O_2 \rightarrow H_2O$ reaction, and a direct methanol cell designed for the $CH_3OH + 3/2\ O_2 \rightarrow 2\ H_2O + CO_2$ process , is characterized by lower efficiency, more complex design and, in addition to water vapor, emits CO_2, which is why it is used to a significantly lesser extent [5]. This makes that molecular hydrogen is usually synonymous with zero-emission energy carrier.

4.1.4.1.1 Methods of obtaining hydrogen

Molecular hydrogen can be obtained from water by splitting it in the process of electrolysis, thermolysis or photolysis, or as a result of biomass gasification, methane pyrolysis, kerosene/oil reforming or in biochemical or photobiological processes [6]. In practice, 96% of global H_2 production comes from coal gasification, hydrocarbon reforming and steam reforming of natural gas [7], even though these methods are energy-intensive and lead to CO_2 emissions. Obtaining molecular hydrogen from water, without CO_2 emissions, is a tempting alternative, but unfortunately also fraught with inconvenience: water thermolysis requires temperatures higher than 2500 K, and photolysis requires far ultraviolet light with a wavelength $\lambda < 186$ nm. Hence, both methods have no practical applications. Water electrolysis, a technique that produces ultra-pure (>99.999%) hydrogen [6], also requires excess energy. Formally, the oxidation potential of water at the anode (reaction $2H_2O \rightarrow O_2$

+ 4 H^+ + 4e^-) under standard conditions at 25 °C is 1.23 V, however, ion diffusion, formation of gas bubbles and other technical factors make it necessary to use higher potentials at limits the energy efficiency of this method and, consequently, its application in the economy. If it is currently widely used, it is only thanks to the use of cheap energy from renewable sources (wind or photovoltaic farms).

4.1.4.1.2 Photoelectrochemical methods of water splitting

The thermodynamic potential of water splitting, 1.23 V, corresponds to the energy of a photon with a wavelength of λ = 1008 nm, the potential increased to values typical in practice, for example 2.0 V, corresponds to the energy of a photon with λ = 620 nm. Therefore, visible light available from the Sun could support the water splitting process, provided a suitable chromophore to absorb light and a catalyst to stimulate the oxidation of H_2O were found. The groundbreaking work of Fujishima and Honda, in which hydrogen was photocatalytically generated from water on a semiconductor electrode (TiO_2) [8], opened a very broad field of research in which systems that operated effectively and for a long time were sought. Unfortunately, today, more than fifty years after the publication of this important work, there are still problems with the stability of materials and low efficiency of the process [9, 10], which is why the photoelectrochemical technique has not been widely used in practice, and the above-mentioned traditional methods are mainly used to obtain hydrogen.

4.1.4.1.3 Hydrogen storage

Typically, molecular hydrogen is stored as a gas compressed to 200-700 bar and this is currently a method commonly used in industry, automotive and other applications [11, 12]. Moreover, it can be stored in liquid form (LH_2) at a temperature reduced to -253 °C, liquid and compressed (cryo-compressed H_2 -CcH_2), as well as using physical or chemical sorption, in metal-organic materials (MOFs) at a temperature of 77 K, in carbon nanostructures, metal hydrates, organic liquids under pressure, or chemically as e.g. methane or ammonia [13, 14]. All these methods have their limitations related to technological complexity, slow hydrogen release or additional energy required to collect or release hydrogen molecules. Hence the popularity of the first solution - storing H_2 in the form of gas in high-pressure cylinders. Such cylinders are used in transport, although a potential collision in road or rail traffic creates the risk of damage, leakage and, consequently, explosion. The awareness of this threat motivates numerous centers looking for new ways of storing hydrogen [14].

4.1.4.1.4 Inspiration from processes occurring in nature

Problems with developing effective and safe methods of obtaining and storing hydrogen have focused researchers' attention on phenomena occurring in nature. In the process of photosynthesis, the energy of the photon absorbed by the chromophore is converted into the chemical energy of the products from the oxidized water: molecular oxygen O_2, H^+ ions and the e^- electron. The ions are transported to the absorbed CO_2 molecules, which are then reduced to organic products [15]. The photosynthetic molecular systems observed in nature are very composite and the processes occurring in them are complex, so their simple replication of them would be very difficult. Therefore, for artificial photosynthesis, it is proposed to create photochemical or photo-electrochemical systems that are significantly simpler than natural ones [16]. In this approach, inspired by nature, the processes would take place in a supra-molecular structure containing organic chromophore molecules acting as a radiation-absorbing antenna and an electron donor and an acceptor [17]. The absorption of a photon by the chromophore would trigger the separation of electric charge leading to the oxidation of the electron donor and the reduction of the electron acceptor located far enough away to make charge recombination impossible [18]. Then the oxidized donor could neutralize OH^- anions and the reduced acceptor could neutralize protons, which would open the way to the recombination of atomic hydrogen into molecular hydrogen [19, 20]. As it turns out, the biggest problem of such a method is the limitation of electric charge recombination, and despite obtaining lifetimes of CT states as long as hundreds of microseconds, H_2 or O_2 have not been obtained directly from H_2O so far [16-20].

Another example of a process commonly occurring in nature is the light-induced joint transfer of an electron and a proton – a process called Proton Coupled Electron Transfer (PCET). PCET is perceived as a mechanism for converting light energy into chemical energy of products that can constitute energy storage, also in the form of molecular hydrogen [21]. However, even in this case, no technology mature enough to be used in practice has yet been developed.

References

[1] Encyclopaedia Britannica, https://www.britannica.com/science/global-warming/Climatic-variation-since-the-last-glaciation

[2] Encyclopaedia Britannica, https://www.britannica.com/science/greenhouse-gas

[3] *A green hydrogen economy for a renewable energy society*, A. M. Oliveira, R. R. Beswick, Y. Yan, *Current Opinion in Chemical Engineering*, 33 (**2021**), 100701

[4] *Methanol as a fuel for internal combustion engines*, S. Verhelst, J. W.G. Turner, L. Sileghem, J. Vancoillie, *Progress in Energy and Combustion Science*, 70 (**2019**) 43–88

[5] *Hydrogen Fuel Cell Vehicles; Current Status and Future Prospect*, Y. Manoharan, S. E. Hosseini, B. Butler, H. Alzhahrani, B. T. Fou Senior, T. A. and J. Krohn, *Appl. Sci.*, 9 (**2019**), 2296

[6] *Renewable hydrogen production*, J. Turner, G. Sverdrup, M. K. Mann, P-Ch. Maness, B. Kroposki, M. Ghirardi, R. J. Evans and D. Blake, *Int. J. Energy Res.*, 32 (**2008**), 379–407

[7] *Methane Pyrolysis for Zero-Emission Hydrogen Production: A Potential Bridge Technology from Fossil Fuels to a Renewable and Sustainable Hydrogen Economy*, N. Sánchez-Bastardo, R. Schlögl and H. Ruland, *Ind. Eng. Chem. Res.,* 60 (**2021**), 11855−11881

[8] *Electrochemical photolysis of water at a semiconductor electrode*, A. Fujishima, K. Honda, *Nature*, 238 (**1972**), 37–38

[9] *Strategies for enhancing the photocurrent, photovoltage, and stability of photoelectrodes for photoelectrochemical water splitting*, W. Yang, R. R. Prabhakar, J. Tan, S. D. Tilley and J. Moon, *Chem. Soc. Rev.*, 48 (**2019**), 4979–5015

[10] *Advanced Catalysts for Photoelectrochemical Water Splitting*, M. A. Marwat, M. Humayun, M. W. Afridi, H. Zhang, M. R. A. Karim, M. Ashtar, M. Usman, S. Waqar, H. Ullah, C. Wang, and W. Luo, *ACS Appl. Energy Mater.*, 4 (**2021**), 12007–12031

[11] *Hydrogen energy, economy and storage: Review and recommendation*, J. O. Abe, A.P.I. Popoola, E. Ajenifuja, O. M. Popoola, *Int. J. Hydr. Ener.*, 44 (**2019**) 15072–15086

[12] *Hydrogen Storage for Mobility: A Review*, E. Rivard, M. Trudeau and K. Zaghib, *Materials*, 12 (**2019**), 1973; doi:10.3390/ma12121973

[13] *Hydrogen Storage in Pure and Boron-Substituted Nanoporous Carbons—Numerical and Experimental Perspective*, L. Firlej, B. Kuchta, K. Walczak and C. Journet, *Nanomaterials*, 11 (**2021**), 2173; doi.org/10.3390/nano11092173

[14] *Hydrogen storage and delivery: Review of the state of the art technologies and risk and reliability analysis*, R. Moradi, K. M. Groth, *Int. J. Hydr. Ener.*, 44 (**2019**), 12254-12269
[15] Encyclopaedia Britannica, https://www.britannica.com/science/photosynthesis
[16] *Mimicking Photosynthetic Solar Energy Transduction*, D. Gust , T. A. Moore and A. L. Moore , *Acc. Chem. Res.*, 34, **(2001)**, 40-48.
[17] *Photoinduced electron transfer in supramolecular systems for artificial photosynthesis*, M. R. Wasielewski, *Chem. Rev.*, 92, **(1992)**, 435-461
[18] *Chemical Approaches to Artificial Photosynthesis. 2*, J. H. Alstrum-Acevedo , M. K. Brennaman and T. J. Meyer , *Inorg. Chem.*, 44, **(2005)**, 6802-6827
[19] *Development of bioinspired artificial photosynthetic systems*, S. Fukuzumi, *Phys. Chem. Chem. Phys.*, 10, **(2008)**, 2283-2297
[20] *Realizing artificial photosynthesis*, D. Gust, T. A. Moore and A. L. Moore, *Faraday Discuss.*, 15, **(2012)**, 9-26
[21] *Proton-Coupled Electron Transfer: The Engine of Energy Conversion and Storage*, Daniel G. Nocera, *J. Am. Chem. Soc.*, 144, (**2022**), 1069−1081

4.1.4.2 Innovative idea - chromophore as a photocatalyst for water splitting

The awareness of the limitations occurring in the photoelectrochemical methods discussed in the introduction led to the thought that the problem of charge recombination, inherent in the ionic path of splitting water or alcohols, does not have to occur in photochemical or photophysical reactions in which radicals are created. In particular, chemists are familiar with molecules called photoacids or photobases, whose acidity or basicity in the excited electronic state increases significantly compared to the values observed for the ground state [1,2]. Pyridine or 1,4-benzoquinone are well-known examples of photobases and it is known that both compounds are photochemically active in protic solvents [3-5]. Such molecular structures are chromophores with a high potential for obtaining hydrogen via the radical pathway [6,7]. It can be expected that for a sufficiently strong photobase X dissolved in water, hydrogen will be separated from the water molecule in the excited state in the processes described by the following equations

$$X + h\nu \rightarrow X^* \qquad (1)$$

$$X^* + H_2O \rightarrow XH\bullet + OH\bullet \qquad (2)$$

In process (2), the energy $h\nu$ of the photon absorbed by the chromophore X is converted into the chemical energy of the photoproducts - the hydrogenated chromophore radical ($XH\bullet$) and the hydroxyl radical ($OH\bullet$). Moreover, it can be expected that the hydrogenated chromophore will behave like a photoacid and, after absorbing another photon, in the excited state the captured hydrogen will be released [7]:

$$XH\bullet + h\nu' \rightarrow X + H\bullet \qquad (3)$$

Hydroxyl radicals generated in reaction (2) may recombine to hydrogen peroxide, H_2O_2

$$OH\bullet + OH\bullet \rightarrow H_2O_2 \qquad (4)$$

and atomic hydrogen obtained in reaction (3) – to molecular hydrogen:

$$H\bullet + H\bullet \rightarrow H_2 \qquad (5)$$

In this way, the absorption of four photons during reactions (1) - (5) would result in the formation of two closed-shell photoproducts H_2O_2 and H_2 and the regeneration of chromophore X, which would be ready for work in the next reaction cycle. The mechanism of four-photon water splitting through the radical path is an alternative to the four-electron splitting of water through the ionic path, traditionally implemented in electrochemical and photoelectrochemical approaches, and has become the subject of a number of theoretical studies by the creators of this concept (A.L. Sobolewski and W. Domcke) [6-8]. Theoretical searches led by them included both organometallic compounds and heterocyclic compounds.

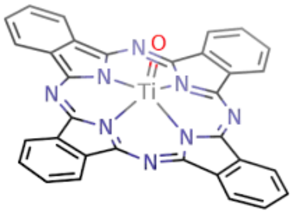

Figure 0. Molecular structure of oxotitanium porphyrin (TiOP).

Historically, the first theoretical studies on the possibility of splitting water with a chromophore performing two functions - a photocatalyst and a "temporary storage" of hydrogen were carried out for the oxotitanyl porphyrin (TiOP) shown in Figure 0 [8]. Calculations of the energy and of the strength oscillator performed for excited electronic states of the isolated TiOP molecule showed the existence of low-lying charge transfer states in which the charge is transferred from the rings of the organic ligand to the *d* orbital of the titanium atom (ligand-to-metal charge transfer state, LMCT). These states, which do not occur in ordinary porphyrin, have a small dipole moment of 1.5 D and a small optical transition oscillator strength of less than 10^{-3}. In the TiOP-H_2O hydrogen-bonded complex, a significant reduction in the energy of the LMCT states (by 0.2 ÷ 0.3 eV) is observed in relation to the optically available states [8]. As a consequence, the dark CT states may be populated as a result of relaxation from the bright, strongly absorbing porphyrin states located above them, responsible for the Soret band of the absorption spectrum of this molecule. Studies of the potential energy surface of the LMCT states of the TiOP-H_2O complex demonstrate their photochemical reactivity and a low barrier in the process of transferring a hydrogen atom from a water molecule to the oxygen atom of the oxotitanyl group of TiOP. As a result, a hydrogen-bonded biradical TiOPH• - OH• is created. Then it may thermodynamically dissociate into two radicals:

$$\text{TiPOH}\bullet\text{–OH}\bullet \rightarrow \text{TiPOH}\bullet + \text{OH}\bullet \qquad (6)$$

The chemical energy of both radicals (~2.6 eV) constitutes a significant part of the energy of the absorbed photon (3.4 eV) [6]. Moreover, a hydrogenated TiOPH• molecule can recombine with another such molecule, releasing hydrogen in an exothermic process (in the gas phase 2.7 kcal/mol) [8]:

$$\text{TiPOH}\bullet + \text{TiPOH}\bullet \rightarrow 2\text{TiPO} + H_2 \qquad (7)$$

The remnant of reaction (6) - two hydroxyl radicals can, also in an exothermic process (in the gas phase 42.9 kcal/mol [8]), recombine to hydrogen peroxide (reaction 4). Moreover, the TiOPH• radical can reduce CO_2 to formic acid HCOOH (exothermally in a gas of 2.5 kcal/mol), expanding the range of possible photochemical processes and their practical applications [8].

Theoretical exploration of the TiPOH• radical revealed the presence of many doublet states with low oscillator strength and optical transition energy corresponding to the visible light region, as well as a strongly absorbing state in UV corresponding to the Soret band of porphyrin. The low-energy excited state of 1^2A_1 having the $\pi\sigma^*$ character has, among other states, an extremely low barrier to dissociation of the OH bond and allows the photodissociation of the hydrogen atom according to reaction (3). Therefore, TiOP theoretically (in the gas phase) enables the implementation of the reaction cycle (1) - (5) leading to the photocatalytic obtaining of molecular hydrogen and hydrogen peroxide from water.

References

[1] *Acid-Base Properties of' Electronically Excited States of Organic Molecules*, *Adv. Phys. Org. Chem.*, J. F. Ireland and P. A. H. Wyatt, 12, **(1976)**, 131-221

[2] *Prototropic equilibria of electronically excited molecules. Part II. 3-, 6-, and 7-Hydroxyquinoline*, S. F. Mason, J. Philp and B. E. Smith, *J. Chem. Soc. A*, **(1968)**, 3051-3056

[3] *Photoactivation of H_20 by p-Benzoquinone and the Role of Mn^{III} Complexes in O_2 Evolution: Molecular Orbital Theory*, M. K. Awad and A. B. Anderson, J. A. C. S., 111, **(1989)**, 802-806

[4] *Mechanism of the photochemistry of p-benzoquinone in aqueous solutions.1. Spin trapping and flash photolysis electron paramagnetic resonance studies*, A. I. Ononye, A. R. McIntosh and J. R. Bolton, *J. Phys. Chem.*, 90, **(1986)**, 6266–6270

[5] *Reversible photolysis of pyridine in aqueous solution*, J. Joussot-Dubien, *Tetrahedron Lett.*, 44, **(1967)**, 4389-4391

[6] *Computational investigation of the photoinduced homolytic dissociation of water in the pyridine–water complex*, Xiaojun Liu , Andrzej L. Sobolewski , Raffaele Borrelli, Wolfgang Domcke, *Phys. Chem. Chem. Phys.*, 15, **(2013)**, 5957–5966

[7] *A computational model of photocatalytic water splitting*, A.L. Sobolewski, W. Domcke, *J. Phys. Chem. A*, 112, **(2008)**, 7311-7313

[8] *Photoinduced water splitting with oxotitanium porphyrin: a computational study*, A. L. Sobolewski and W. Domcke, *Phys. Chem. Chem. Phys.*, 14, **(2012)**, 12807–12817

4.1.4.3 Experimental verification of the new concept of splitting water and methanol - discussion of the results of work P1–P5

Below are short presentations of the works that constitute the habilitation achievement. The articles are presented in chronological order to better show subsequent issues and problems occurring in experimental research, as well as to illustrate the progress that has been achieved in understanding the mechanism of photocatalytic extraction and storage of hydrogen from protic liquids. The descriptions of the results do not contain literature references, as they are included in the content of the articles discussed.

4.1.4.3.1 Publication P1 – the first experimental evidence of water oxidation via the radical pathway

Achievement: using oxotitanium tetraphenylporphyrin as a photocatalyst, hydroxyl radicals were obtained from water.

For the first attempts at photocatalytic water oxidation, oxotitanium tetraphenylporphyrin (TiPPO, Figure 1) was used instead of the previously theoretically explored oxotitanyl porphyrin (TiOP), because it is more chemically stable, forms hydrogen bonds with water and, thanks to its extensive structure, has a main absorption band (Soret) in the visible region (Figure 2), which enables the possible use of this molecule for practical applications.

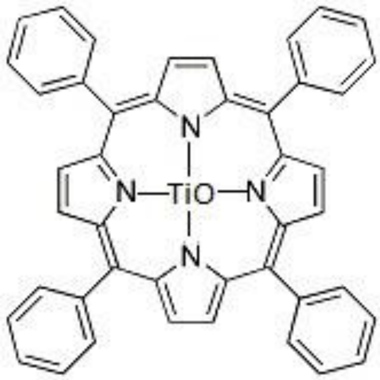

Figure 1. Molecular structure of TiPPO.

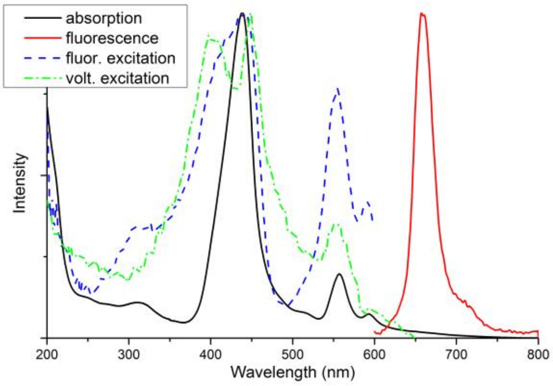

Figure 2. Absorption, emission, fluorescence and photo-current excitation spectra of TiPPO on a plate in water.

Calculations performed using the TD-DFT method for the TiPPO molecule show the existence of two optically accessible (optical transition oscillator strength f > 0) electronically excited states of the $\pi\pi^*$ character and two "dark" (f = 0) states with charge transfer from the ligand to the metal (LMCT) with a πd character (Table 1). Since the most absorbing *B* band (Soret) has an excitation energy higher than the states with charge transfer from the ligand to the metal, LMCT states can be populated when excited to the *B* band by non-radiative relaxation. The theoretical results (Table 1) are qualitatively consistent with the experimental results (Figure 2). Calculations for the complex with the TiPPO---H_2O hydrogen bond show that the order of states in the complex remains similar and the LMCT states are located between the "bright" $\pi\pi^*$ states. Moreover, exploration of the potential energy surface of LMCT states shows a low barrier to the hydrogen atom transfer process and the possibility of creating biradicals in these states in the reaction: TiPPO---H_2O → TiPPOH•---HO• (state diagram in Table 1). Hence, TiPPO is a good candidate to act as a water splitting photocatalyst.

Table 1. Energies (ΔE) and oscillator strength (f) of the lowest excited electronic states of TiPPO and the state diagram of the TiPPO---H_2O complex obtained from TD-DFT calculations.

State	ΔE/eV (λ/nm)	f	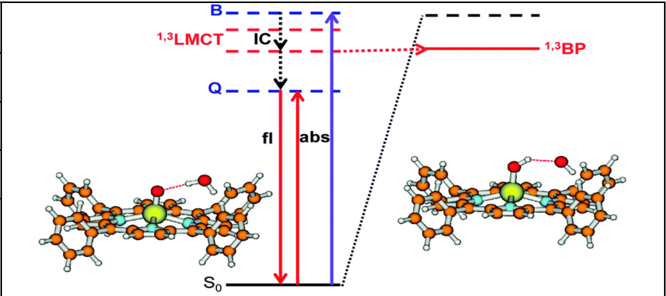
$^{1}\pi_{P}\pi^{*}_{P}$(Q)	2.29(546)	0.11×10^{-2}	
$^{1}\pi_{P}d_{Ti}$(CT)	2.76(453)	0.0	
$^{1}\pi_{P}d_{Ti}$(CT)	3.01(415)	0.0	
$^{1}\pi_{P}\pi^{*}_{P}$(B)	3.21(390)	2.13	

TiPPO is not water-soluble, so quartz plates with a deposited molecular layer up to 20 nm thick were used for optical studies whereas for photo-current measurements the molecular material was deposited on flat electrodes coated with gold. It was expected that irradiation of TiPPO layer plates immersed in water with light of wavelength corresponding to the B-band (Soret) would lead to the formation of biradicals which would then dissociate to form two photoproducts: the hydroxyl radical OH• and the hydrogenated oxotitanyl tetra-phenyl-porphyrin TiPPOH•. Both open-shell systems are reactive and can form further chemical compounds, adding to the complexity of the issue, and it was therefore decided to detect the presence of hydroxyl radicals as the first and obvious products of the photocatalytic water splitting reaction. For this purpose, the known method of chemical dosimetry was used. In this method, molecules that undergo hydroxylation change their optical properties are used as detectors, so that by observing changes in the absorption or emission spectra, the presence of hydroxyl radicals in solution can be detected. In this study, two radical scavengers were used as 'sensors' of hydroxyl radicals - terephthalic acid (TA), which upon OH• attachment converts to hydroxyterephthalic acid (HTA) showing strong fluorescence, and benzoic acid (BA) that upon hydroxylation converts to fluorescent salicylic acid (SA).

TiPPO molecular layers immersed in water with TA (pH = 11.5) or with BA (pH = 7.0) were irradiated with a blue light laser, observing in both cases the increase in fluorescence of the hydroxylated forms (Figure 3). In this way, experimental evidence was obtained for the generation of radicals in alkaline and neutral water and, indirectly, for the photocatalytic water splitting reaction:

$$\text{TiPPO} + h\nu \rightarrow \text{TiPPO}^* \qquad (1)$$

$$\text{TiPPO}^* + H_2O \rightarrow \text{TiPPOH}\bullet + \text{OH}\bullet \qquad (2)$$

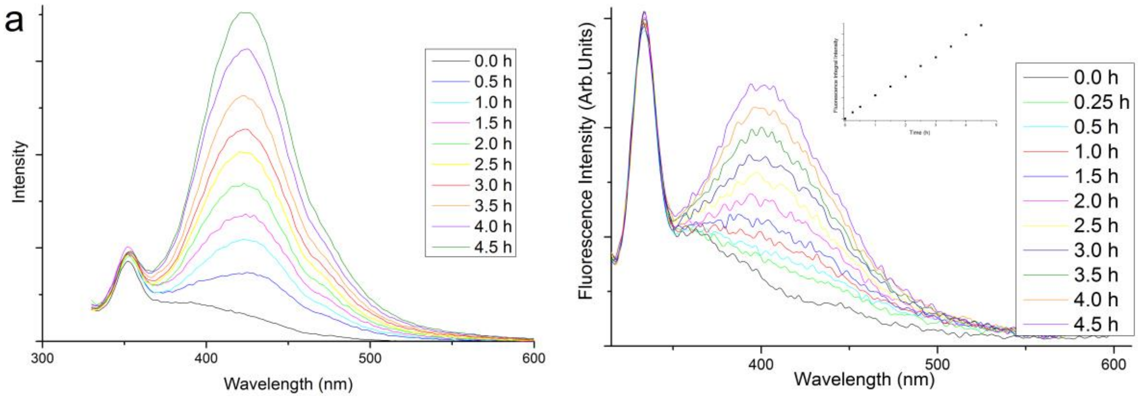

Figure 3. Increase of HTA (left) and of SA fluorescence (right) in result of 445 nm laser irradiation of TiPPO plates in base water with TA and neat water with BA acid respectively.

Irradiation of the chromophore in small-volume cuvettes made it possible to determine the quantum yields of the photochemical reaction, which turned out to be small, on the order of a few per milles only (Table 2).

Table 2. Quantum efficiency and HTA concentration increase rate constant.

Initial TA concentration [M]	Laser power [mW]	Efficiency	HTA build-up rate [M/s]
$4.78*10^{-4}$	30	3.07×10^{-3}	7.08×10^{-7}
$4.78*10^{-4}$	50	4.11×10^{-3}	1.56×10^{-6}
$4.70*10^{-4}$	50	4.33×10^{-3}	1.66×10^{-6}
$4.78*10^{-4}$	70	5.32×10^{-3}	2.60×10^{-6}

In addition to the photocatalytic generation of radicals, photoinduced generation of electric charges was observed, and the excitation spectrum of photocurrent in water is similar to the excitation spectrum of fluorescence (Figure 2), suggesting that the formation of ions is related to the population of CT states of the hydrogen bond TiPPO-water complex. The irradiation of TiPPO molecules in water leads thus to an ionic pathway described by the equation

$$\text{TiPPO}^* + H_2O \rightarrow \text{TiPPOH}^+ + \text{OH}^- \qquad (3)$$

Measurements of the electric current in a closed circuit and the voltage obtained in an open circuit as well as the efficiency of the ion generation process are presented in Table 3. It is clearly visible that a small photovoltaic effect is characterized by very low efficiency. Comparing it with the efficiency of radical generation shows that the radical pathway (equation 2) is three orders of magnitude more efficient than the ionic pathway described by equation (3). This result supports the concept of photocatalytic water splitting via the radical path and indicates the accuracy of the theoretical calculations carried out for the reactions occurring in the excited states of the hydrogen bonded complex.

Table 3. Parameters of the TiPPO ion path in water.

Wavelength [nm]	V_{oc} [V]	I_{sc} [μA]	Efficiency
445	0.26	0.1	4.6×10^{-6}
570	0.24	0.11	2.4×10^{-6}

It was also noticed that few hours long photoirradiation of the molecular layer in water leads to complete degradation of this layer. The probable cause is the attack of hydroxyl radicals on the extensive molecular structure of TiPPO. This observation indicates a weak point of the radical pathway water splitting method and its possible limitations in the use of the chromophore over time.

Individual contributions from authors:

O. Morawski (55%) - definition of the research concept and the scope of experimental work, measurements of optical spectra and electrical waveforms, preparation of results, text of the article
K. Izdebska (5%) – operating a vacuum evaporation machine to get molecular layers
E. Karpiuk (5%) – performing some optical measurements (HTA fluorescence spectra)
J. Nowacki (5%) – synthesis of molecular material (TiPPO)
A.Suchocki (5%) – providing a vacuum evaporation machine, discussions about work
A. L. Sobolewski (25%) – proposing a topic, theoretical calculations, tables and figures with theoretical results, description of theoretical results, editing the text of the article

4.1.4.3.2 Publication P2 – confirmation of the mechanism of photocatalytic water oxidation

Achievement: it was shown that photocatalytic oxidation of water requires the population of LMCT charge transfer states, thus confirming their reactivity indicated by the theory

Titanyl phthalocyanine (TiOPc, Figure 4) was used as a catalyst in the tests. The molecule can be synthesized in a simple way, is commercially available and is widely used in toners for laser printers. It has a strong absorption band (Q) in the red and near infrared region and a Soret absorption band (B) in the near ultraviolet (Figure 5). The presence of an intense absorption band in the near infrared and red region potentially creates the possibility of using a significant part of the solar radiation spectrum for photocatalysis.

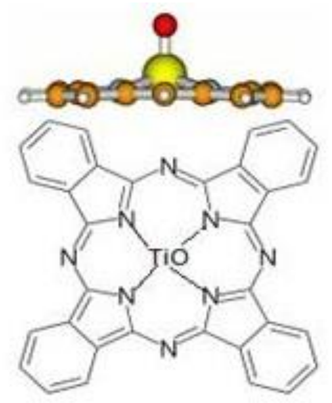

Figure 4. Molecular structure excitation of TiOPc.

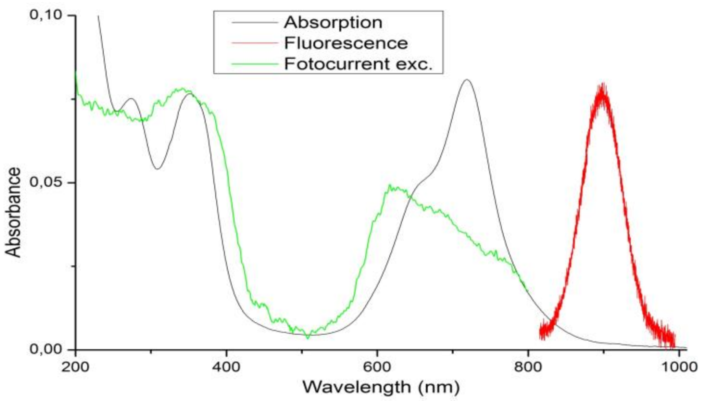

Figure 5. Absorption, fluorescence and photocurrent spectra of TiOPc on plate in water.

Calculations carried out using quantum chemical methods indicate the similarity of the order of the excited electronic states of TiOPc and TiPPO. In titanyl phthalocyanine, the lowest singlet (1^1E) has the $\pi\pi^*$ character and high oscillator strength, above it there is the dark LMCT state (π*d*Ti) and significantly the next $\pi\pi^*$ state also with zero oscillator strength (Table 4). Only at 1.64 eV above the S_1 (visible in the absorption band as the Q band) there is a strongly absorbing state of the $\pi\pi^*$ character, which is responsible for the B (Soret) band of the absorption spectra identified in the near UV (Figure 5). This location of electronic states distinguishes TiOPc from TiPPO. In TiOPc the energy difference between the lowest singlet and the next S_n absorbing state (2^1E) is much greater than in TiPPO, and the difference between the S_n absorbing state and the LMCT state is also greater, amounting to 1.3 and 0.5 eV in both molecules, respectively. (see tables 1 and 4). This means that if, as a result of non-radiative relaxation, the LMCT state is populated from the optically excited S_n (2^1E) state, it has a greater excess of vibrational energy. Calculations for the TiOPc---H_2O complex show that the order and energy distances of the states do not change significantly and the process of transferring the hydrogen atom from water to the oxygen atom of the titanyl group is exothermic (Figure 6). In contrast, in the lowest energy state $S_1(\pi\pi^*)$ (1^1E), this process is endothermic (Figure 6).

Table 4. Energy (ΔE) and oscillator strength (f) of the lowest singlets of TiOPc.

State	ΔE\eV	f
$^1\pi\pi^*$	2.02	0.75
$^1\pi d_{Ti}$	2.36	0.0
$^1\pi\pi^*$	3.27	0.0
$^1\pi\pi^*$	3.58	0.20
$^1\pi\pi^*$	3.66	0.90

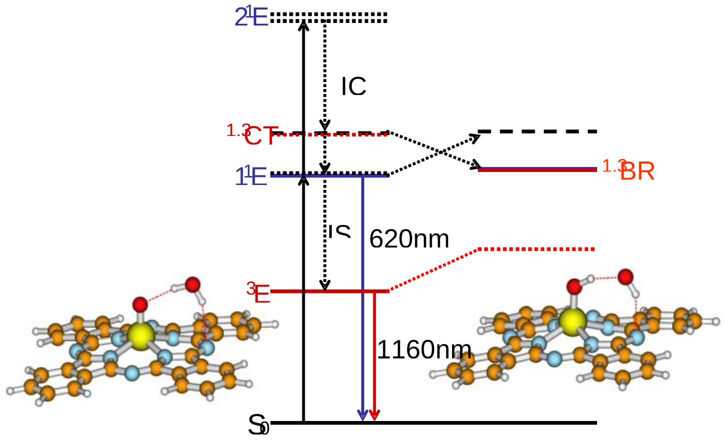

Figure 6. Schema of electronic states of TiOPc---H_2O obtained with TD-DFT method.

TiOPc dissolves very poorly in water and was evaporated onto quartz plates for optical measurements and onto gold electrodes for current measurements. Similarly to TiPPO, a chemical dosimetry method with terephthalic and benzoic acid as a radical scavenger and a fluorescent OH• radical probe was used to detect hydroxyl radicals. Occurrence of photocatalytic reaction

$$\mathrm{TiOPc}^{*} + H_2O \rightarrow \mathrm{TiOPcH}\bullet + \mathrm{OH}\bullet \tag{4}$$

was checked both with optical excitation to the lowest S_1 singlet (Q band of the absorption spectrum) and to the high S_n singlet (the Soret B band). It turned out that process (4) occurs only with high-energy excitation (Figure 7). (The residual build-up of HTA luminescence seen in Figure 7b comes from excitation of the aqueous solution with the 315 nm light used to excite the HTA. It is also absorbed by the high singlet states of TiOPc, from which reactive LMCT states could be populated.) This result confirms the theoretical model that predicts that LMCT is the reactive state and it must be populated for the photocatalytic water splitting reaction to occur. This is only feasible from the higher state S_n. The LMCT (πdTi) state cannot be thermally populated by S_1 excitation because it is 0.34 eV lower than the LMCT state and at room temperature $kT = 0.026$ eV << 0.34 eV. With the excitation within the Soret band, process (4) also occurs not only in alkaline water but also in neutral water at pH = 7.0. Hence "tuning" the pH does not affect the radical pathway, which contrasts with photoelectrochemical methods.

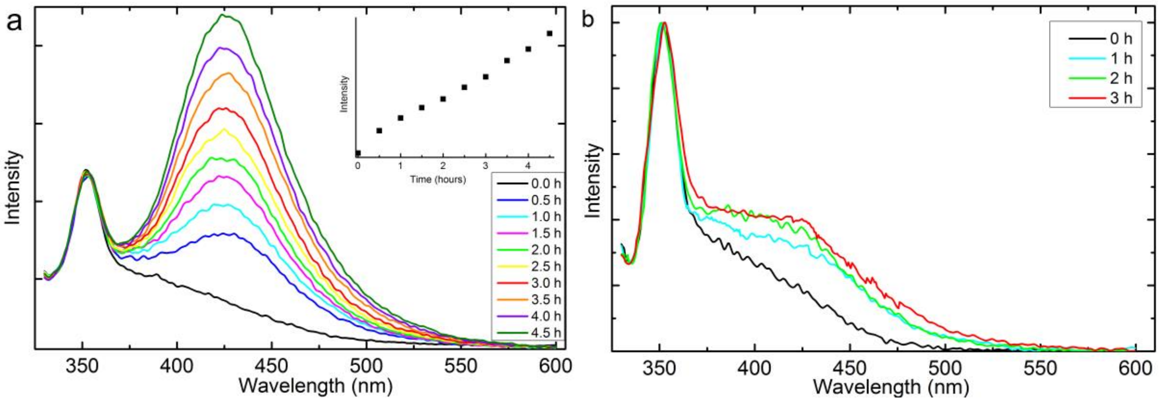

Figure 7. Effect of irradiation of TiOPc w alkaline water (pH = 11.5) on HTA fluorescence. Irradiation within: (a) (Soret) B band and (b) Q band. HTA fluorescence spectra recorded with 315 nm excitation.

Studies on the kinetics of the conversion of TA acid to the hydroxylated form of HTA (Figure 8) made it possible to determine the reaction rate constants and process efficiency (Table 5). The efficiencies of photocatalytic generation of hydroxyl radicals by TiOPc are higher than the values obtained for TiPPO. The higher process efficiency in TiOPc is associated with the large excess energy obtained in this molecule thanks to the greater energy separation between the states: absorbing Sn($\pi\pi^*$) and reactive LMCT(πdTi).

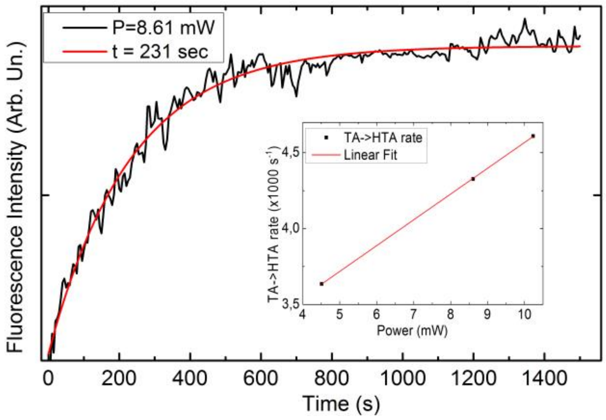

Figure 8. Effect of TiOPc irradiation (λ = 315 nm, P = 8.61 mW) on HTA fluorescence. Inset illustrates linear dependence of rate constant on laser power.

Table 5. Efficiency and rate constant of hydroxylation process TA → HTA for TiOPc.

Light power [mW]	Efficiency	HTA build-up rate [M/s]
4.51	0.16	1.8×10^{-6}
8.61	0.14	2.0×10^{-6}
10.23	0.13	2.1×10^{-6}

For TiOPc in water, a weak photovoltaic effect is observed and the photocurrent excitation spectrum is similar to the absorption spectrum (Figure 5). Time measurements of electrical waveforms for alternating light/dark cycles of the chromophore show the generation and slow recombination of electric charges in water (Figure 9). However, very low intensity of electric current and efficiencies of this process are obtained (Table 6), which means that the ionic path is practically irrelevant.

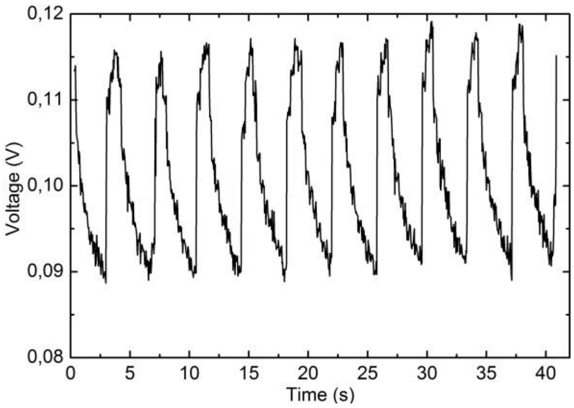

Figure 9. Photovoltaic effect for TiOPc in water with (short) cycles of irradiation and (longer) cycles in dark of TiOPc molecular layer in water.

Table 6. Photovoltaic parameters for TiOPc in water.

λ_{exc} [nm]	power [mW]	V_{oc} [V]	I_{sc} [μA]	efficiency
405	75	0.12	0.06	3×10^{-6}
660	66	0.12	0.05	1.5×10^{-6}
730	75	0.11	0.02	4.6×10^{-7}
800	264	0.11	0.02	1.5×10^{-7}

Similarly to TiPPO, it was noticed that exposure of the TiOPc molecular layer in water for several hours of irradiation leads to its significant degradation and this was associated with the presence of hydroxyl radicals produced in the photocatalytic process.

Indywidualny wkład autorów:
O. Morawski (55%) – concept of the research, scope of experimental work, measurements of optical spectra and electrical waveforms, preparation of results, text of the article
K. Izdebska (5%) – operating a vacuum evaporation machine to get molecular layers
E. Karpiuk (5%) – performing some optical measurements (HTA fluorescence spectra)
Y. Zhydachevskyy (10%) – operation of the Fluorolog-3 spectrofluorimeter
A. Suchocki (5%) – providing a vacuum evaporation machine, discussions about work
A. L. Sobolewski (20%) – theoretical calculations, tables and figures with theoretical results, editing the theoretical part of the article text.

4.1.4.3.3 Search for new chromophores - unpublished research

The detection of hydroxyl radicals produced photo-catalytically in water by TiPPO and TiOPc was a partial success only, because no detection of the hydrogenated chromophore was achieved, and in particular, no changes were observed in their absorption spectrum. This was due to the use in molecular tests of layers of water-insoluble TiPPO and TiOPc molecules, which are photo-catalytically active only on their surface, so the strong absorption of the entire layer may mask the weak absorption of hydrogenated molecules located on its surface. Therefore, research work was performed on a number of organic molecules soluble in water and absorbing light in the visible range, such as methylene blue or acridine orange, for which preliminary theoretical calculations indicated that they could enable photocatalytic water splitting. Experimental studies have generally failed to confirm theoretical predictions for these structures.

The second problem considered was the photo-degradation of the chromophores used in the water splitting study caused by reaction with hydroxyl radicals generated during the process. This phenomenon is related to the high redox potential of the hydroxyl radical, 2.8 V, which is one of the highest in nature. Only molecular fluorine (F_2) has a higher potential value, 3.03 V, and generally known active oxidants such as ozone (O_3), hydrogen peroxide (H_2O_2) or chlorine (Cl_2) have lower potential values - 2.07, 1.78 and 1.36 V respectively. Hence the very high reactivity of OH• radicals and the rapid hydroxylation of the chromophore leading to its significant degradation. In this aspect, alcohols are an alternative to water: they are also protic and, like water, form hydrogen bonds with azaaromatic molecules. However, their radicals have lower potentials, e.g. for methoxy ($CH_3O\bullet$) and ethoxy ($C_2H_5O\bullet$) it is 0.73 and 0.69 V, respectively, which means that they can be expected to influence the degradation of the photocatalyst molecule to a lesser extent or slower. Moreover, organic molecules usually dissolve better in alcohols than in water, creating solutions that enable the use of various experimental techniques.

4.1.4.3.4 Publication P3 – HATN – chromophore with properties desirable for photocatalysis

<u>Achievement</u>: *explanation of the photophysics of the hexaazatrinaphthylene molecule (HATN) in solvents, determining the impact of aggregation on photophysics and recognizing the photochemical process occurring in methanol*

Photophysics studies of the hexaazatrinaphthylene molecule (HATN, Figure 10) were undertaken due to its interesting properties - an extensive structure potentially offering absorption in the near UV or even visible region of the spectrum, and the presence of six nitrogens in the rings that could provide it with the characteristics of a strong photobase. A number of works were found in the literature in which the use of HATN derivatives was proposed, including lithium-ion batteries, as molecules enabling the creation of energy stores with a high electron storage density.

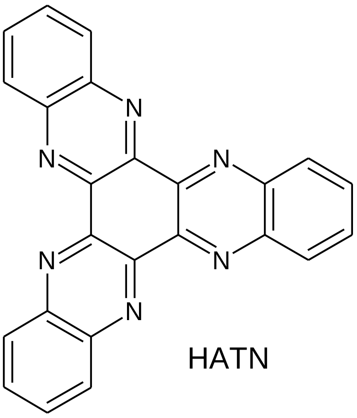

HATN

Figure 10. Molecular structure of hexaazatrinaphthylene (HATN).

Quantum chemical calculations performed using the ADC(2)/cc-pVDZ method for the geometry of the ground state of the molecule optimized using the MP2/cc-pVDZ method showed that the lowest singlet state is nπ.* (Table 7). Slightly above there are optically available states of the ππ* character. Taking into account the fact that the ADC(2) method overestimates the energies of the states by approximately 0.4 eV, we can expect absorption to occur close to the border of the visible part of the electromagnetic spectrum. The calculations also reveal the degeneracy of the excited electronic states related to the C_3 symmetry of the molecule.

Table 7. Energy (ΔE), oscillator strength (f) and dipole moment (μ), of HATN lowest excited singlets.

State	ΔE/eV	f	μ/D
S_0	0.0	-	0.0
^{3}ππ*	2.80	-	0.0
^{3}ππ*	2.98	-	1.24
^{3}ππ*	2.98	-	-1.24
^{3}nπ*	2.99	-	-0.51
^{3}nπ*	2.99	-	0.51
^{3}nπ*	3.08	-	0.0
^{1}nπ*	3.41	0.0	-0.63
^{1}nπ*	3.41	0.0	0.63
^{1}nπ*	3.50	0.0	0.0
^{1}ππ*	3.70	0.0	0.0
^{1}ππ*	3.71	0.211	0.97
^{1}ππ*	3.71	0.211	-0.97
^{1}ππ*	3.94	0.0	0.0
^{1}ππ*	4.14	0.057	4.18
^{1}ππ*	4.14	0.057	-4.18
^{1}ππ*	4.45	0.0	0.0
^{1}ππ*	4.58	1.621	3.76
^{1}ππ*	4.58	1.621	-3.76

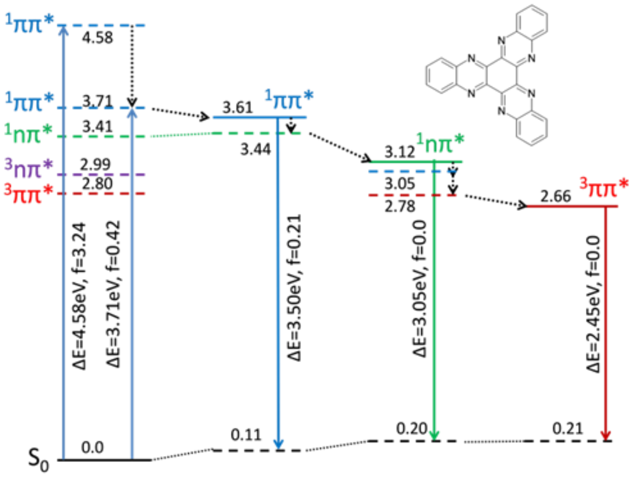

Figure 11. Jabłoński scheme and photophysics of HATN. Adiabatic states (optimized) are denoted with solid line. With broken line denoted states obtained in geometry of optimized states. Solid and broken arrows denote radiative and non-radiative transitions. Multiplicity and character of states is presented with color. Numbers specifies relative energy expressed in electrovolts.

Below the singlet states there are triplet states of the nπ* and $\pi\pi$* nature. Therefore, efficient intersystem crossing to the triplet manifold $^1\pi\pi^* \rightarrow {}^3n\pi^*$ and $^1n\pi^* \rightarrow {}^3\pi\pi^*$ should be expected, as illustrated in Figure 11, and, consequently, weak $S_1(n\pi^*) \rightarrow S_0$ fluorescence. Experimental data confirm these predictions - the absorption spectrum starts already in the visible region (Figure 12) and fluorescence spectra are of very low intensity (Figure 13). The slight solvatochromism of the spectra confirms small changes in the dipole moment of electronic states.

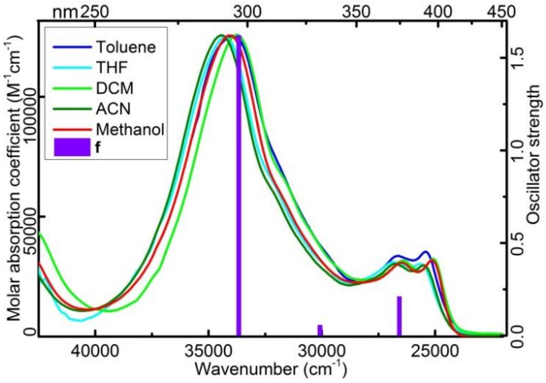

Figure 12. Absorpction spectra of HATN in solvents and oscillator strength (f). Energy of transitions decreased by 0.4 eV.

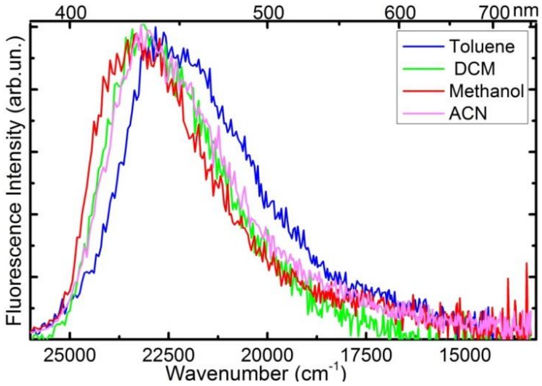

Figure 13. Fluorescencce spectra of HATN in solvents.

Table 8. Fluorescence quantum yield Φ_F, triplet formation efficiency Φ_T, fluorescence decay time τ_F, and rate constants of the transitions: radiative k_r, intersystem k_{isc} and non-radiative k_{nr}, for HATN in solvents at T = 298 K.

Solvent	Φ_F	Φ_T	τ_F	k_r	k_{isc}	Φ_{nr}	k_{nr}
	$\times 10^{-4}$	$\times 1$	ps	10^7 s^{-1}	10^9 s^{-1}	$\times 1$	10^9 s^{-1}
Toluene	4.8	0.32	77	0.62	4.2	0.68	8.8
DCM	7.3	0.41	50	1.46	8.2	0.59	11.8
Methanol	2.6	0.21	15	1.85	15.0	0.79	56.4

Low fluorescence quantum yields and emission decay times of the order of tens of picoseconds (Table 8) are typical for heterocyclic molecules with the lowest excited singlet state of nπ* character and are associated with high efficiency of the intersystem transition to triplet states, which is also observed for HATN (table 8, Φ_T, k_{isc}). However, the dominant relaxation channel at room temperature is internal conversion (k_{nr}). At cryogenic temperatures, it slows down and at T = 5 K the HATN emission spectrum is dominated by phosphorescence, the intensity of which is several times higher than that of fluorescence. To sum up, the photophysics of the HATN monomer is relatively simple and the results of theoretical calculations and experimental studies consistently indicate the nπ* nature of the lowest excited singlet state. Moreover, a significant increase in the rate constant of non-radiative transitions is observed in methanol, which may indicate the existence of an optical excitation relaxation channel other than internal conversion. The extensive and flat molecular structure of HATN facilitates the formation of aggregates. Dimer formation occurs already at low chromophore concentrations, on the order of tens of micromoles per liter, and manifests itself as a new band on the long-wave side of the emission spectrum (Figure 14). The changes in the absorption spectrum are smaller, indicating the formation of H-type aggregates in which the optical transition is allowed only to the higher state of the aggregate and the lower state is optically dark. The long fluorescence decay time of the dimer (2.3 ns in dichloromethane) confirms this assumption. In the powder and both obtained crystal structures, the fluorescence decay times are even longer and the spectra are more red-shifted, providing further justification for the nature of the states and interactions in HATN aggregates.

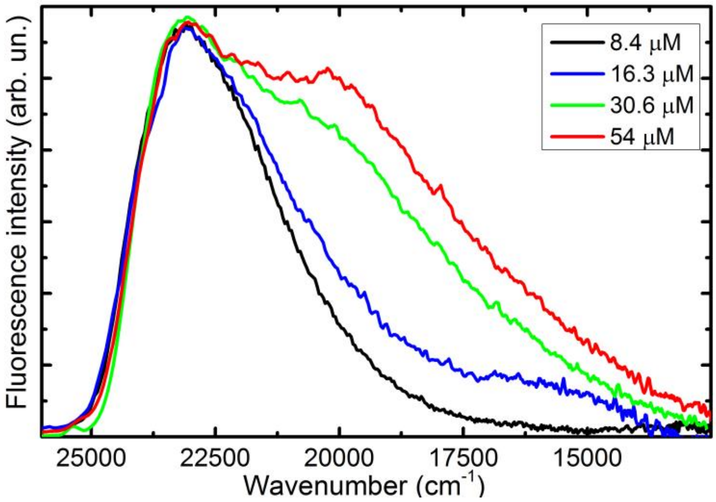

Figure 14. Fluorescence spectra of HATN in DCM at selected concentrations.

Individual contributions from authors:

Olaf Morawski (60%) – defining the research concept and the scope of experimental work, measuring optical spectra and kinetics for all phases (liquid, powder, crystal structures), developing the results, writing the text of the article

Jerzy Karpiuk (10%) – performing microsecond transient absorption measurements of HATN in solvents, determining the triplet formation efficiency and decay times of triplet states at room temperature and editing the text of the article

Paweł Gawryś (10%) – synthesis of the molecular material (HATN)

Andrzej L. Sobolewski (20%) – theoretical calculations, tables and figures with theoretical results, editing the text of the article

4.1.4.3.5 Publication P4 – detection of hydrogenated chromophore

<u>Achievement</u>: clear experimental evidence confirming the process of photochemical hydrogen storage on the hexaazatrinaphthylene molecule

In the work P3 it was shown that the lowest excited singlet state of HATN has an nπ^* character and can be formed by relaxation from higher $\pi\pi^*$ states absorbing visible light, and that a photochemical reaction takes place in methanol. Publication P4 contains the results of a number of studies using optical methods, electron paramagnetic resonance (EPR), nuclear magnetic resonance (NMR) and mass spectroscopy (MS) of HATN in methanol, carried out to explain the mechanism and identify the products of this reaction.

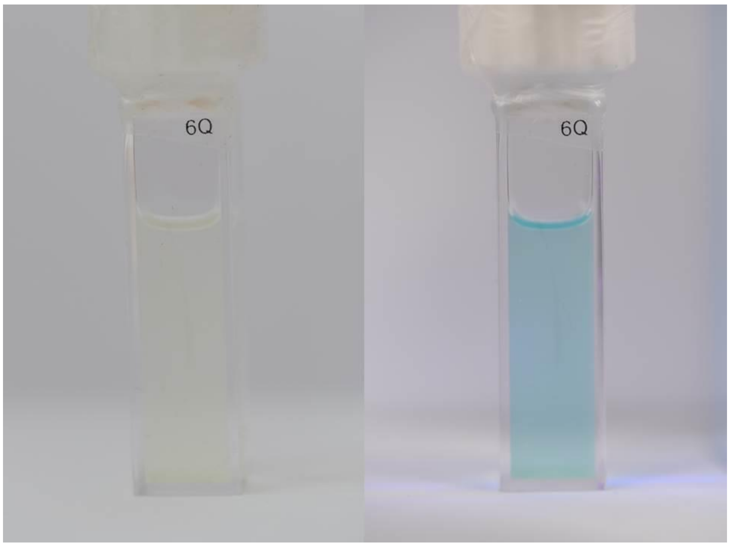

Figure 15. HATN in methanol solution irradiated with 405nm laser becomes colored to blue.

Irradiation the cuvette with the degassed HATN solution in methanol with a several milli watts 405 nm laser leads to the blue colorization of the solution (Figure 15). In anaerobic conditions, the color may last for months. Comparison of the absorption spectra before and after irradiation shows that new bands are created with a maximum at 1.78 and 3.9 eV, while the absorbance of the HATN spectrum decreases (Figure 16a). The difference between these spectra (Figure 16b) represents the spectrum of photoproducts formed as a result of irradiating the solution. It is similar to the absorption spectrum of doubly hydrogenated HATN (HATN-2H) obtained in calculations carried out using various methods (Figure 17), which suggests that such a closed-shell molecular system is the final product of the photochemical reaction of HATN in methanol.

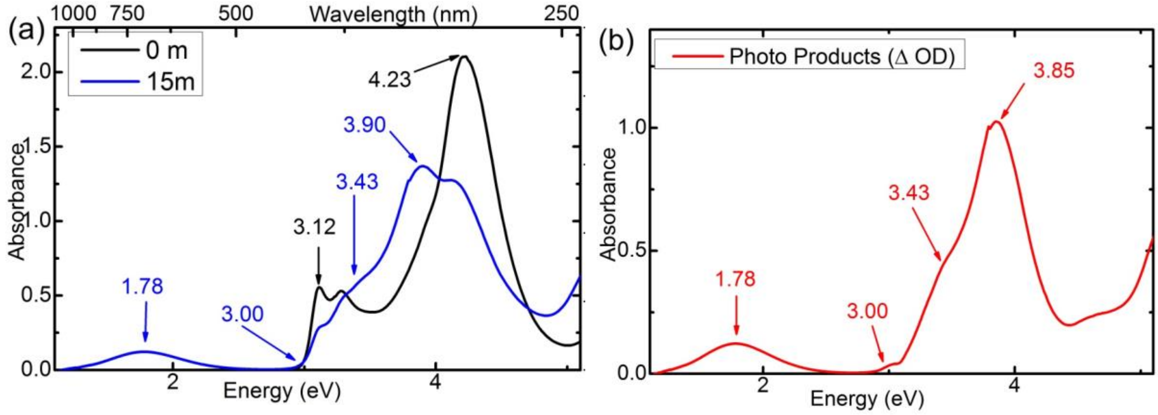

Figure 16. (a) Absorption spectra of methanol solution of HATN before and after 15 minutes of photoiradiation with 405 nm laser, (b) difference between „before" and "after" irradiation absorption spectra.

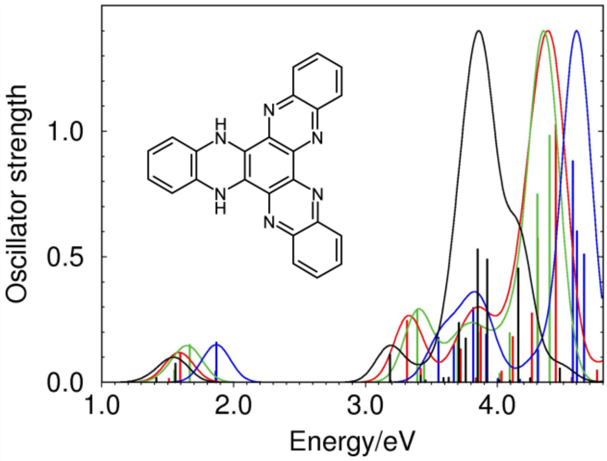

Figure 17. Absorption spectrum of di-hydrogenated HATN obtained with different methods: TD-DFT (black), ADC(2) (red), CC2 (green) and SCS-CC2 (blue), resulted from the convolution of discrete theoretical spectra with Gauss curve of 0.25 eV width.

Theoretical exploration of the hydrogen-bonded complex of HATN with a methanol molecule shows that the lowest excited singlet state is nπ* and is a state with charge transfer (CT). This is clearly indicated by the Natural Transition Orbitals (NTOs, table 9), which show that in the CT(nπ*) state electron density is transferred from the n orbital of the nitrogen and methanol atoms to the HATN rings, while in the LE(ππ) state there is a redistribution of the electron density only on the HATN rings. Hence, it can be expected that in the CT state jump of methanol's electron onto nitrogen atom will be followed by transfer of proton from the hydroxyl group of methanol. Figure 18, presenting the energy profile of states as a function of the OH bond length, illustrates that such an assumption is probable and the process may take place in the CT(nπ*) state, as the energy of this state decreases with the increase in the O-H bond length in methanol.

Table 9. Natural Transition Orbitals for LE(ππ∗) and CT(nπ∗) states of HATN-CH_3OH complex obtained with ADC(2) method.

State	hole	electron
LE(ππ*)	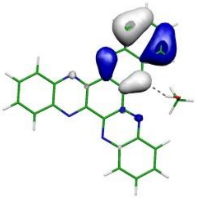	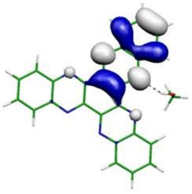
CT(nπ*)	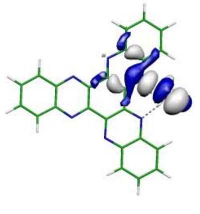	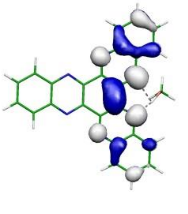

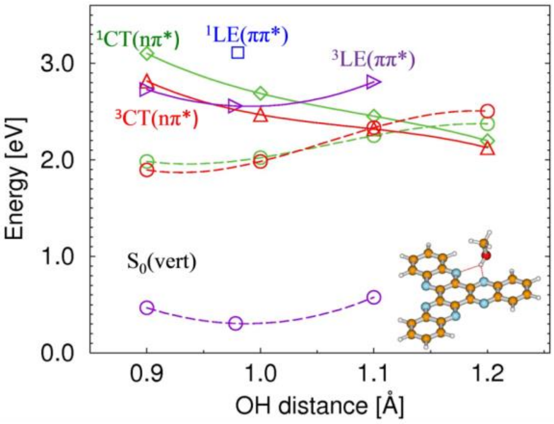

Figure 18. Energy in function of OH distance for electronic states of HATN-$HOCH_3$ complex: $^1\pi\pi^*$- blue squares, $^1n\pi^*$- green rhombs, $^3\pi\pi^*$- violet triangles, $^3n\pi^*$- red triangles. S_0 energy calculated for geometry of given excited state, as pointed by the color, is labeled by circles.

As a result, we can talk about coupled electron and proton transfer (PCET) from methanol to the nitrogen atom of the HATN molecule. Fluorescence decays in methanol-h_4 and deuterated methanol-d_4 (Figure 19) show a lengthening of the lifetime of the excited state from $\tau_F(H)$ = 18 ps to $\tau_F(D)$ = 28 ps, thus proving that in the excited state of the complex a hydrogen atom is transferred. Since in non-protic solvents PCET does not occur and $1/\tau_F = k_r + k_{nr} + k_{isc}$, then the constants can be calculated from the decay times in methanol where $1/\tau_F = k_r + k_{nr} + k_{isc} + k_{PCET}$. So determined hydrogen atom transfer rate in ordinary and deuterated methanol is $k_{PCET}(H) = 4.3\times10^{10}\ s^{-1}$ and $k^{PCET}(D) = 2.3\times10^{10}\ s^{-1}$ respectively. The obtained values are typical for this process and prove that the HATN hydrogenation process takes place in the lowest energetically excited singlet state of the HATN-methanol complex and are a clear experimental confirmation of the theoretical model.

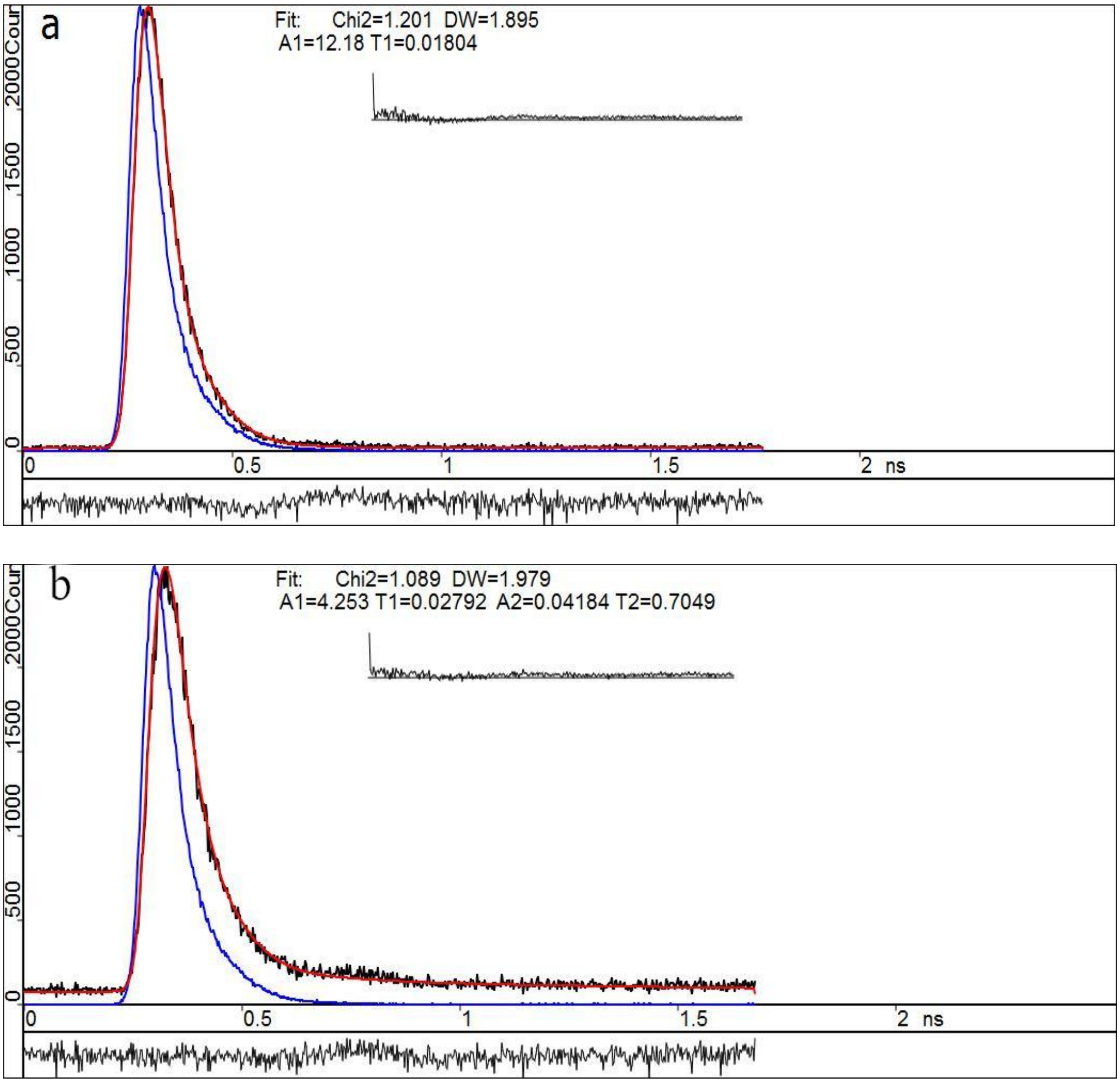

Figure 19. Fluorescence decay traces observed at 428 nm (black), excitation pulses 388.5 nm (blue) and fluorescence decay traces obtained from deconvolution program (red) of HATN in **CH_3OH** (a) and **CD_3OD** (b). Traces recorded with 814 fs per channel resolution. In deuterated methanol the presence of the second decay component of small amplitude (1%) can be assign to emission from HATN dimers.

In result of photocatalytic hydrogenation of HATN in w methanol (5)

$$\mathrm{HATN} + h\nu + \mathrm{CH_3OH} \rightarrow \mathrm{HATNH}\bullet + \mathrm{CH_3O}\bullet \qquad (5)$$

two radicals are formed: methoxy and hydrogenated HATNH•. Confirmation of the generation of radicals was obtained in EPR measurements of the HANT solution in methanol before and after irradiation (Figure 20). A weak EPR signal indicates a low concentration of radicals and an efficient recombination process. Indeed, the fluorescence spectra presented in Figure 21 prove that the methoxylation process of HATN and coumarin takes place during irradiation of the solutions.

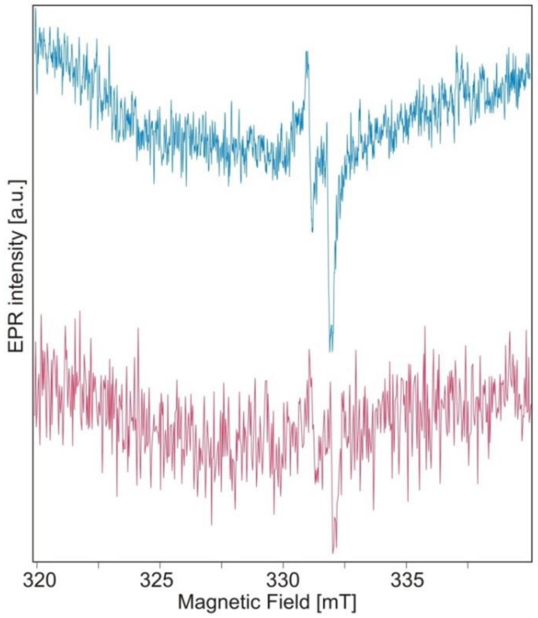

Figure 20. EPR spectra of HATN in methanol before (red) and after (blue line) 405 nm laser irradiation. Spectra recorded at T=100 K, irradiation performed at temperature 20°C.

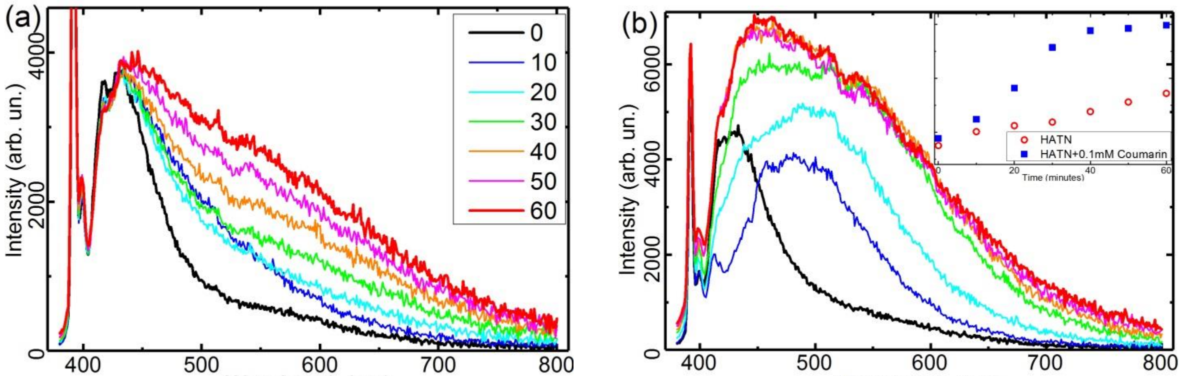

Figure 21. Fluorescence spectra of HATN methanol solution irradiated with 405nm laser recorded at 10 minutes intervals (a), and of HATN with 0.1 mM coumarin in methanol (b). Excitation at 340 nm. The legend in (a) specifies time of irradiation and color of the spectrum, inset in (b) depicts integral intensity of HATN fluorescence spectra (red) and HATN with 0.1 mM coumarin (blue squares) in function of time of irradiation. The narrow band at 392 nm is a Raman line of methanol.

The ^1H NMR spectrum shows that when irradiating HATN in methanol with violet light, the intensity of the chromophore bands decreases, and at the same time new bands appear and grow. This means that the concentration of substrates (HATN) decreases and the concentration of photoproducts increases with exposure time (Figure 22). The width of the photoproduct bands makes it impossible to analyze their molecular structure, and another experimental technique is required to analyze the newly formed structures.

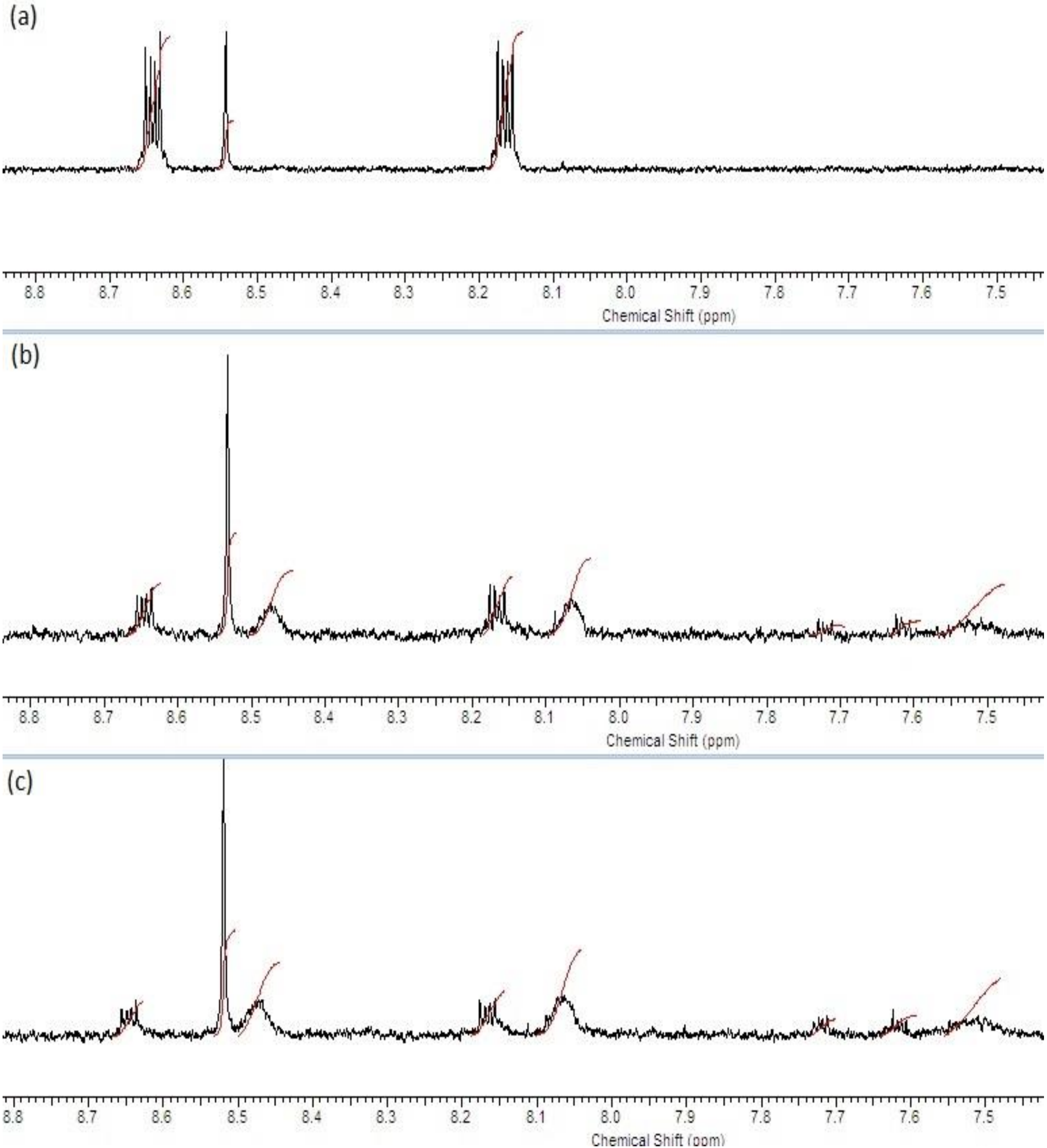

Figure 22. ^1H NMR spectra of HATN in deuterated methanol (CD_3OD) (a) before irradiation, (b) after 5 minutes and (c) after 10 minutes of 405 nm laser irradiation. Note that vertical scale of (a) differs from (b) and (c). Red curves represent integral intensity of spectra bands.

In order to identify photoproducts, high-resolution mass spectroscopy (HR MS) was used, ensuring oxygen-free conditions during the measurement. Comparison of the mass spectrum obtained before irradiation (Figure 23) with the spectrum after irradiation (Figure 24) illustrates that the vast majority of HATN molecules observed on line 407.1 convert to doubly hydrogenated $HATNH_2$ from line 409.12.

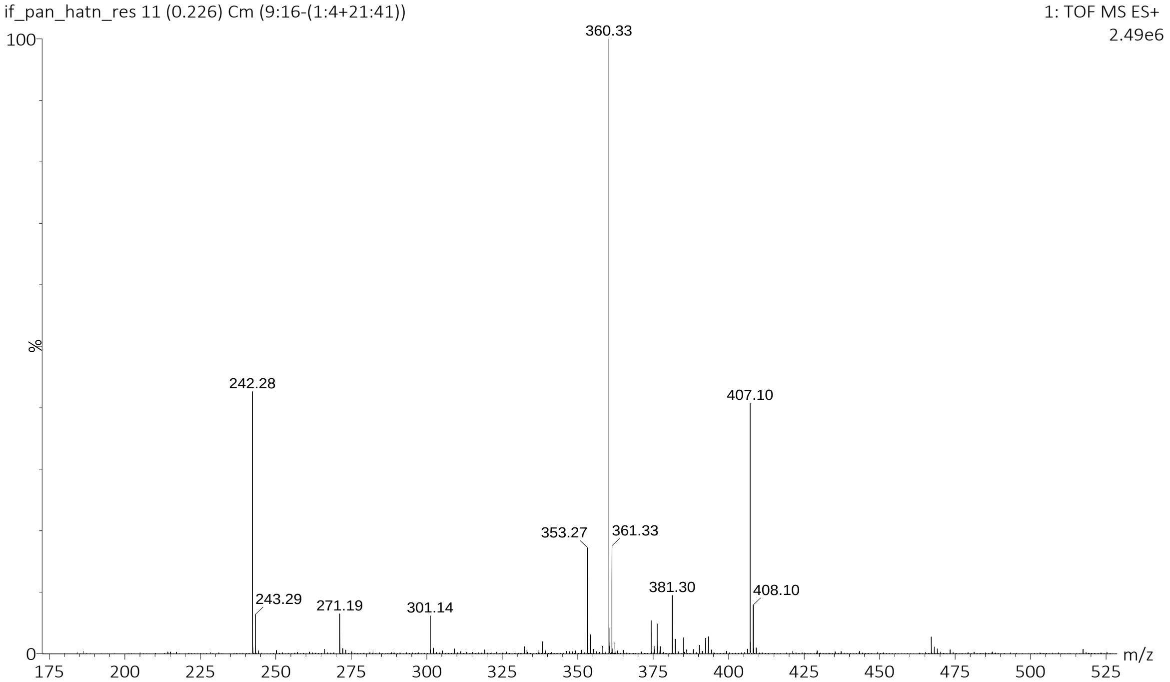

Figure 23. Mass spectrum with HATN with sodium ion line at $m/z = 407.10$ $[HATN+Na]^+$.

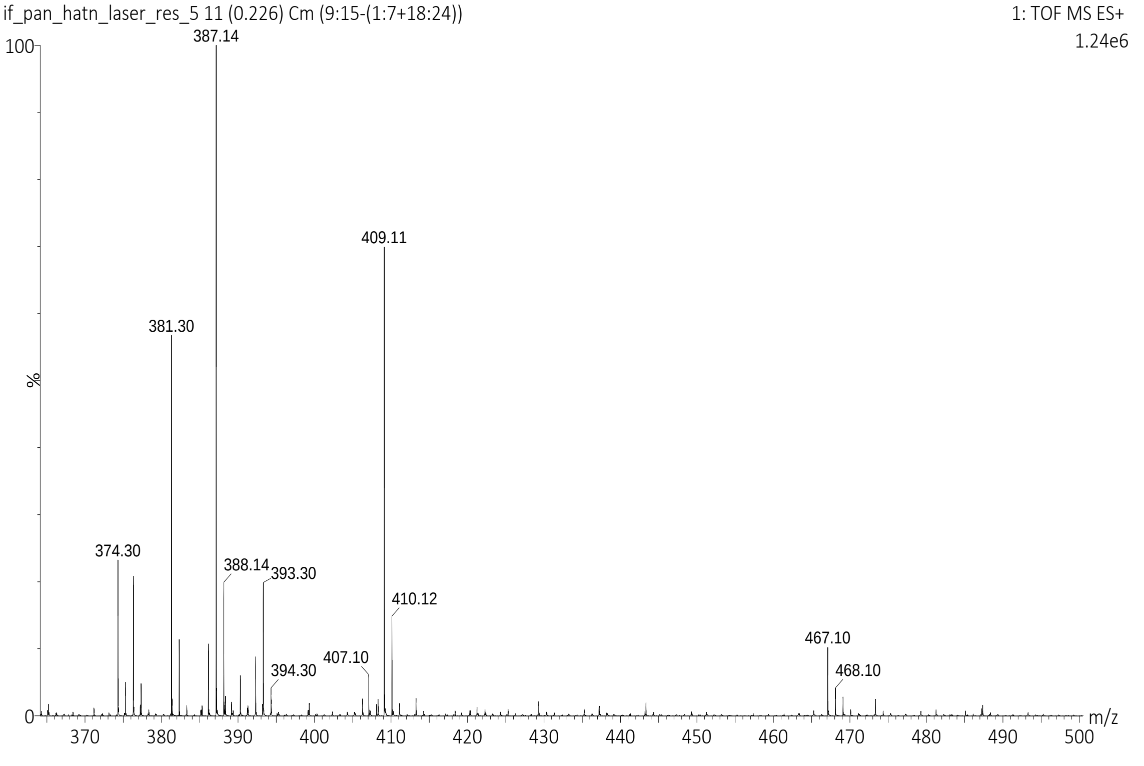

Figure 24. Mass spectrum with $HATNH_2$ with sodium ion line at $m/z = 409.12$ $[(HATN+2H)+Na]^+$.

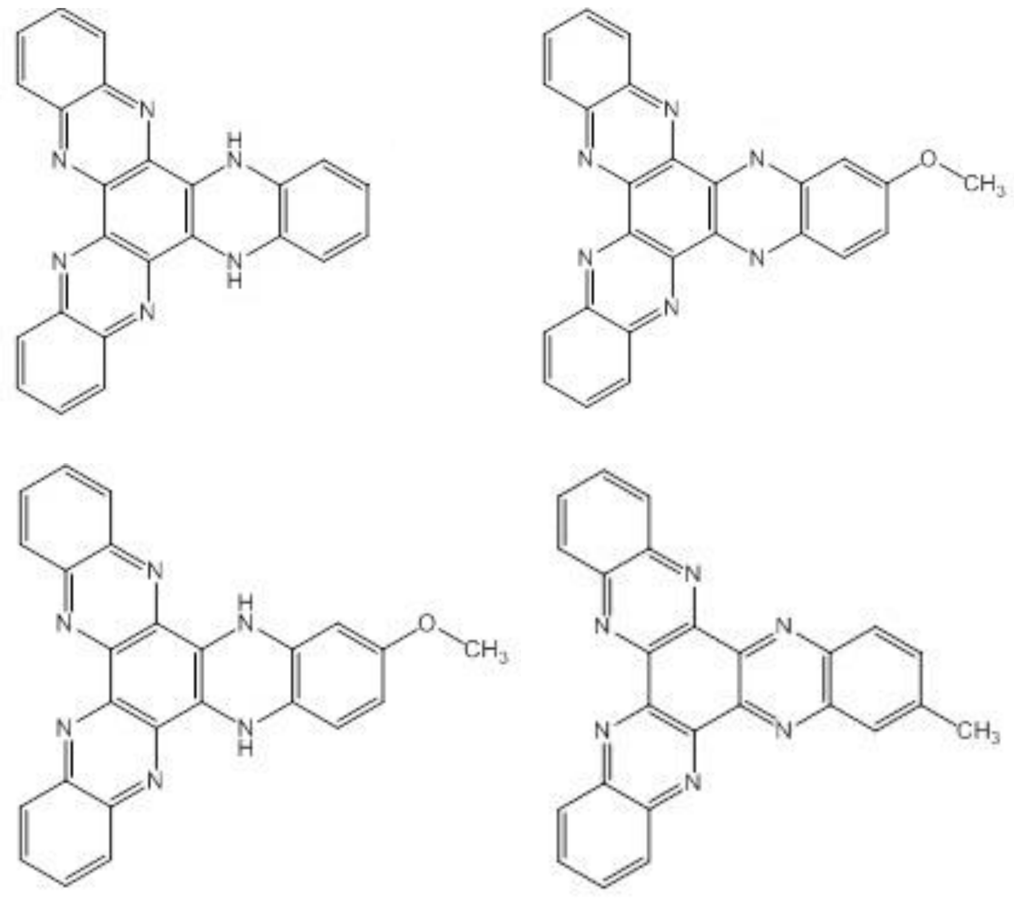

Figure 25. Molecular structures of HATN main photoproducts proposed for mass spectroscopy results . Positions of the groups are ambiguous.

Together with the doubly hydrogenated HATN molecule, its methoxylated and methylated structures are observed (Figure 25), which confirms the attack of methoxyl radicals on this chromophore. With longer exposures, double hydrogenated and methoxylated structures also occur. This is good news - the reaction with a radical does not necessarily mean the loss of a hydrogen atom or methoxylation does not destroy the photocatalytic properties of the chromophore. Therefore, HATN can act as a photocatalyst and hydrogen storage despite reacting with radicals.

In addition to doubly hydrogenated HATN monomers ($HATNH_2$), hydrogenated dimers ($HATN_2H_2$ and $HATN_2H_4$) and trimers ($HATN_3H_2$, $HATN_3H_4$ and $HATN_3H_6$) were also observed in the mass spectra. This result shows that high-density hydrogen storage is possible. However, no HATN structures hydrogenated more than twice were observed, which was initially expected when the structure with six nitrogen atoms was selected for research. The release of hydrogens from the chromophore is achieved by reaction with oxygen. The $HATNH_2$ oxidation process then takes place in the reaction

$$\mathrm{HATNH_2 + HATNH_2 + O_2 \rightarrow 2HATN + 2H_2O} \qquad (6)$$

which proceeds spontaneously and, as shown by calculations carried out using the D3-DFT/B3-LYP/cc-pVDZ method, is exothermic - its enthalpy is $\Delta E = -70.4$ kcal/mol (3.05 eV), which gives -17.5 kcal/mol (0.76 eV) on a hydrogen atom. Reaction (6) proves that doubly hydrogenated HATN is a molecule storing chemical energy that can potentially be released through the use of a properly selected catalyst or used in an appropriate fuel cell. In anaerobic conditions, this energy can be stored long-term, it has been verified that even longer than one year.

Individual contributions from authors:

Olaf Morawski (65%) – defining the scope of experimental work, coordinating (outside the IF PAN) and conducting research, measuring optical spectra and fluorescence kinetics, preparing the results, writing the text of the article

Paweł Gawryś (10%) – synthesis of molecular material (HATN), cyclic voltammetry measurements.

Jarosław Sadło (Institute of Nuclear Chemistry and Technology) (10%) – EPR spectra measurements

Andrzej L. Sobolewski (15%) – theoretical calculations, tables and figures with theoretical results, editing the text of the article

NMR and HRMS spectra measurements were performed as a paid service provided with the participation and supervision of OM at the Faculty of Chemistry of the University of Warsaw (NMR) and at the Institute of Organic Chemistry of the Polish Academy of Sciences in Warsaw (HRMS). EPR spectra have been recorded by Jarosław Sadło at Institute of Nuclear Chemistry and Technology in Warsaw with some support from OM.

Awards

The article was featured:

1. Cover Feature:

DOI: 10.1002/cphc.202200316

2. From a note on the Chemistry Views website (this is the online scientific news magazine of Chemistry Europe, an organization of 16 European national chemical societies):

https://www.chemistryviews.org/hydrogen-storage-with-hexaazatrinaphthylene/

3. Mention on Twitter (currently X):

https://twitter.com/ChemistryViews/status/1519144691131846656

4.1.4.3.6 Publication P5 – photocatalytic hydrogenation of aza-arenes

<u>Achievement</u>: experimental confirmation of the possibility of photochemical hydrogen storage with quinoxaline derivatives, determining of a relation between the chromophore structure and its stability and suitability for obtaining and storing hydrogen.

Studies of the photophysics and photochemistry of three quinoxaline derivatives, tentatively named PQPhen, PQ2Py and Q2Py, having three, four and five nitrogen atoms, respectively, and slightly different molecular structures (Figure 26) were performed in publication P5. The research was carried out in terms of their suitability for obtaining and storing hydrogen and resistance to attack by radicals generated during the oxidation of methanol.

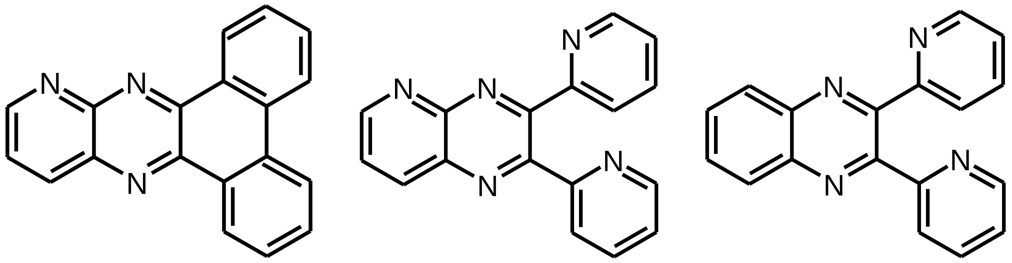

PQPhen PQ2Py Q2Py

Figure 26. Molecular structure of PQPhen, PQ2Py and Q2Py.

The fundamental difference between the ground state molecules is the planarity of PQPhen and the contrasting twists of the pyridine rings in PQ2Py and Q2Py (Figure 27). Cyclic voltammetry in acetonitrile showed that the molecules have similar redox properties, and reversible protonation was observed for them in protic methanol. PQ2Py and Q2Py powders are white, suggesting UV absorption, while the yellow color of PQPhen powder indicates visible light absorption. All molecules were known before, but none of them had been tested for photophysical processes, so measurements of the absorption, emission and fluorescence decay spectra of these chromophores in various solvents were carried out. Quantum chemical calculations showed that in all molecules the lowest singlet excited state is nπ*, so very weak emission was expected in all solvents and in protic solvents - the PCET process and photochemical accumulation of hydrogen.

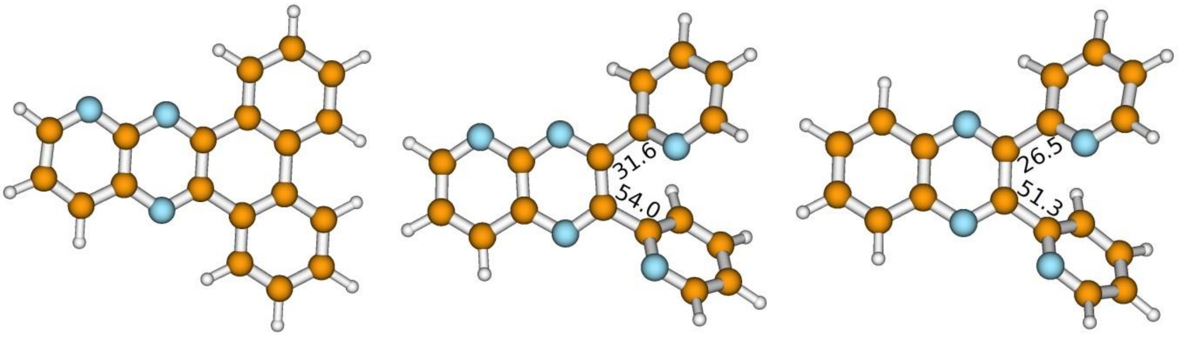

Figure 27. Ground state molecular structures of PQPhen, PQ2Py and Q2Py molecules optimized by the MP2/cc-pVDZ method. To emphasize the non-planarity of PQ2Py and Q2Py, numbers representing the values of the dihedral angles NCCC and CCCC are given.

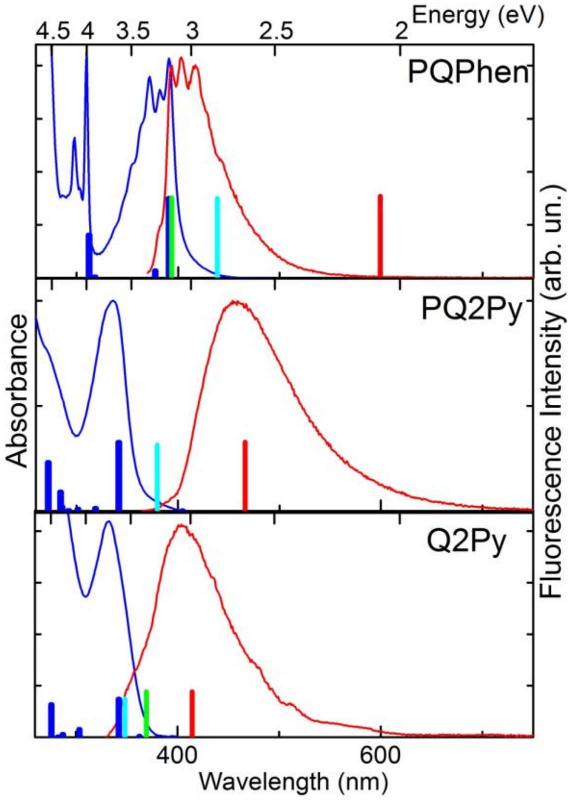

Table 10. Fluorescence quantum yield, Φ_F, decaytime, τ_F, radiative, k_r, and nonradiative, k_{nr}, rate constants of chromophors in solvents.

	Solvent	Φ_F/%	τ_F /ps	k_r [$10^7 s^{-1}$]	k_{nr} [$10^9 s^{-1}$]
PQPhen	n-hexan	2.7	180	15.0	5.4
	ACN	0.11	120	0.9	8.3
	MeOH	0.9	26	3.4	38.1
PQ2PY	n-hexan	0.25	200	1.25	5.0
	ACN	0.05	150	0.03	6.7
	MeOH	0.11	51	2.16	19.6
	H_2O	0.09	550	0.16	1.82
Q2PY	n-hexan	0.012	46	0.26	21.7
	ACN	0.005	40	0.13	25.0
	MeOH	0.007	45	0.16	22.2
	H_2O	0.022	206	0.11	4.85

Figure 28. Absorption and fluorescence spectra in *n*-hexane and theoretical energy and oscillator strength of transitions (vertical bars): absorption (blue – $\pi\pi^*$, magenta – $n\pi^*$), emission (green – $\pi\pi^*$, red– $n\pi^*$).

As expected, PQPhen, with the most extensive molecular structure, absorbs light already in the visible region at 410 nm, and PQ2Py and Q2Py molecules - in the UV. Moreover, PQPhen has a very small Stokes shift and clearly stronger emission than the other two chromophores, in which the rotation of the pyridine rings can lead to a change in the geometry of the molecule in the excited state, lowering the energy of the excited state and increasing the rate constant of non-radiative transitions. The Φ_F and τ_F values observed for PQ2Py and Q2Py (Table 10) are typical for the $^1n\pi^*$ states what together with the large Stokes shift prove that these molecules undergo relaxation from the absorbing $^1\pi\pi^*$ state to the lowest and low-emission state $^1n\pi^*$. The minimal Stokes shift observed for PQPhen in n-hexane and the mirror symmetry of the absorption and fluorescence spectra indicate that the emission comes from the absorbing $^1\pi\pi^*$ state. This is a surprising result because calculations show that also in PQPhen the lowest excited singlet state is $n\pi^*$ and the absorbing $^1\pi\pi^*$ state should be 0.4 eV higher (Figure 28). Emission from the $S_2(\pi\pi^*)$ state means that Kasha's rule is violated in PQPhen, which states that fluorescence comes from the lowest excited singlet state. The case of PQPhen is strange, because the law of the energy gap for internal conversion would suggest that with such a small (0.4 eV) difference in the energies of the $S_2(\pi\pi^*)$ and $S_1(n\pi^*)$ states, efficient $S_2 \rightarrow S_1$ non-radiative relaxation should occur in this molecule. The explanation of the anomalous fluorescence comes from the analysis of the molecular structure of PQPhen and its symmetry. The chromophore is flat and the mixing of (orthogonal) electronic states $S_2(\pi\pi^*)$ - $S_1(n\pi^*)$ can only be caused by out-of-plane C-H vibrations. However, in PQPhen all hydrogen atoms are distant from nitrogen atoms and therefore the overlap of n and π orbitals is small. Hence, in this flat molecule, the interaction of the $S_2(\pi\pi^*)$ - $S_1(n\pi^*)$ states is very weak and the internal conversion, despite the small energy gap between them, is ineffective. In protic methanol, complexes with a PQPhen-MeOH hydrogen bond are formed, the symmetry of such a molecular system decreases, and mixing of electronic states becomes possible. In methanol, the fluorescence spectrum undergoes a strong red shift and the Stokes shift increases up to 0.5 eV. This and the short fluorescence decay time and its low quantum yield (Table 10) prove that the non-radiative relaxation $S_2(\pi\pi^*) \rightarrow S_1(n\pi^*)$ is effective and the emission occurs from the lowest excited state of $n\pi^*$ character.

The photocatalytic properties of chromophores were tested by irradiating their degassed solutions in methanol with light of the appropriate wavelength: 405 nm for PQPhen, 375 nm for PQ2Py and 277 nm for Q2Py. The formation of photoproducts and the possibility of hydrogenation of molecules were checked by examining their absorption spectra before and after irradiation and after oxygenation of the solution (Figure 29). Changes in the absorption spectra of solutions after irradiation reveal the generation of photoproducts. Oxygenation of the solution with PQPhen photoproducts causes the changes in the spectrum to reverse and its shape almost returns to its original one. Such changes, analogous to those observed for HATN, suggest hydrogenation of PQPhen is reversible in contact with O_2. For PQ2Py this is observed to a significantly lesser extent, and for Q2Py - to a minimal extent, which suggests that both of these chromophores undergo permanent transformation or degradation during the photocatalytic process.

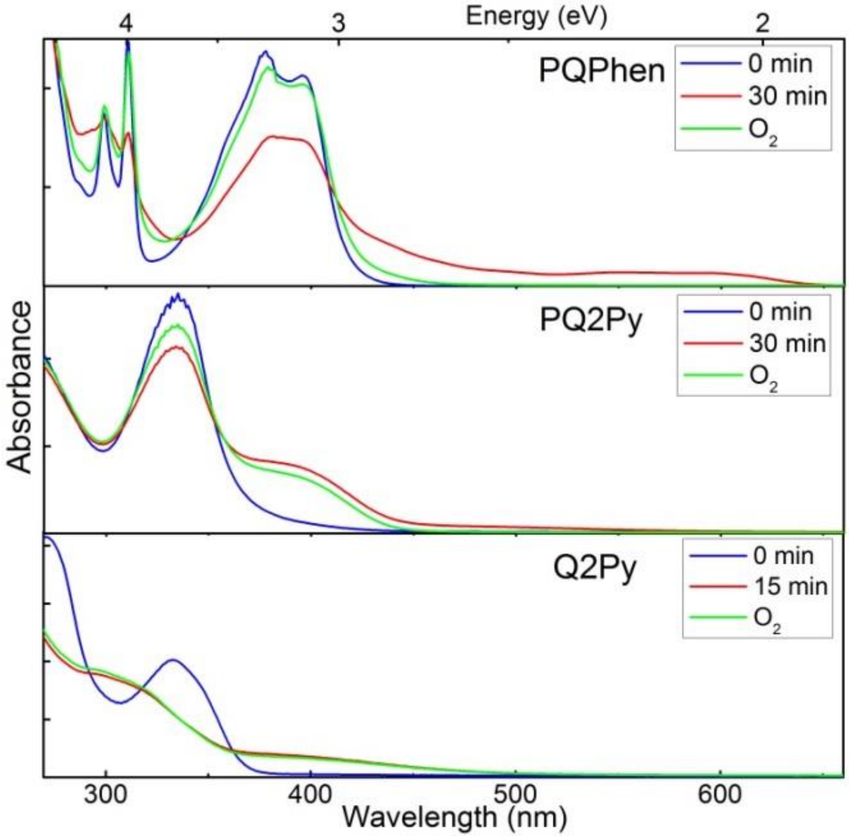

Figure 29. Absorption spectra of PQPhen, PQ2Py and Q2Py in degassed methanol before (blue), after irradiation (red) and after injecting oxygen (green lines).

The formation of some photoproducts can be monitored in luminescence during irradiation of solutions of chromophores in methanol (Figure 30). The fluorescence of the photoproducts is always much more intense than the luminescence of the chromophores, which indicates a change in the nature of the emission state. Two fluorescent photoproducts are observed for PQPhen and Q2Py, and one for PQ2Py. PQ2Py and Q2Py photoproducts are stable even when oxygen is introduced into the solution. All products are stable under anaerobic conditions and can be tested using other experimental techniques.

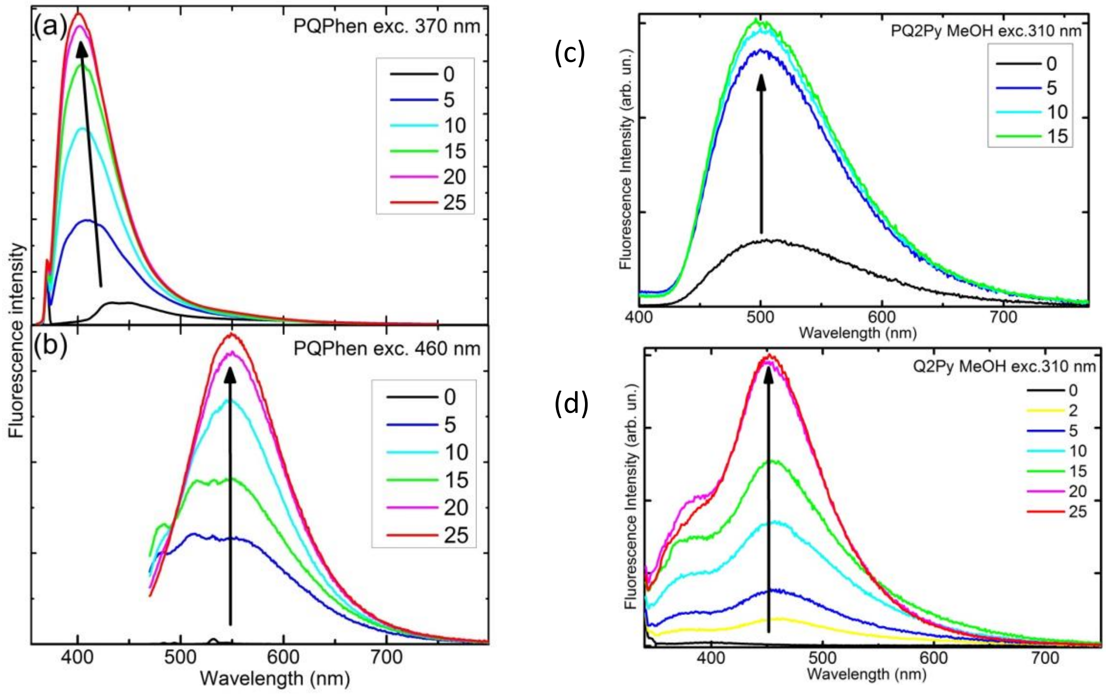

Figure 30. Fluorescence spectra of photoproducts formed in solutions as a result of irradiation. The legends indicate the color of the spectrum observed after the exposure time expressed in minutes.

EPR measurements of solutions after irradiation did not show the presence of radicals. This suggests their rapid recombination, including reaction with the chromophore. It must be efficient because the use of coumarin in the solution as a scavenger of methoxyl radicals to protect PQPhen against methoxylation is only effective at very high concentrations. This is illustrated in Figure 31, which shows, up to the 50th minute of exposure, in addition to the fluorescence of methoxylated coumarin (maximum at 410 nm), the contribution from the fluorescence spectrum of PQPhen. At lower coumarin concentrations, only photo-products of PQPhen are observed.

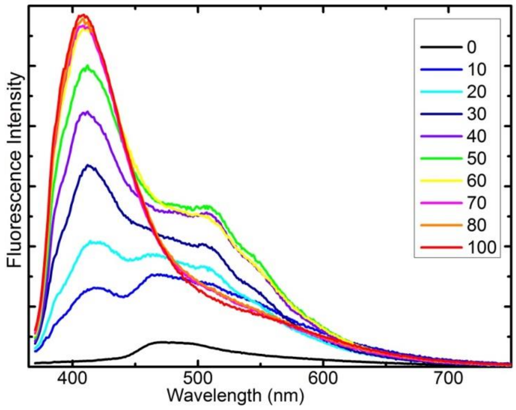

Figure 31. Fluorescence spectra of PQPhen with 0.5 M coumarin solution. Legend specifies time of 405 nm laser irradiation in minutes.

For all chromophores, the formation of photoproducts can be monitored by nuclear magnetic resonance, NMR. Even a short (5 minutes) irradiation of the PQ2Py solution in methanol-d_4 causes numerous changes in the NMR spectrum of hydrogen (^1H). In addition to new bands formed in the area of 7.3 - 9.3 ppm, bands in the range of 2.5 - 4.0 ppm are also formed (spectra are not shown here, can be found in SI of **P5**), proving the generation of photoproducts with alkyl groups created in a result of the opening of aromatic rings. This phenomenon may occur during multiple methoxylation or methylation of the aromatic ring.

High-resolution mass spectroscopy (HRMS) spectra enable very accurate indication of the masses of photoproducts, which enables indirect determination of their molecular structure. For PQPhen, comparison of mass spectra of solutions before and after irradiation proves that irradiation leads to the formation of hydrogenated and methoxylated PQPhen and hydrogenated and methylated PQPhen (the spectra are not shown here, they are found in SI of paper **P5**). PQPhen photoproducts always have masses higher than PQPhen, which indicates that methanol fission products - hydrogen and methoxy or methyl groups - are attached to the chromophore, as shown in Figure 32 presenting the proposed structures for the masses of photoproducts most frequently occurring in the HRMS spectrum. The presence of such structures shows that the attack of methoxy radicals does not interfere with the hydrogenation of the chromophore, and the doubly hydrogenated PQPhen is a stable molecular system capable of storing hydrogen even despite the reactivity of some radicals. At the same time, the occurrence of these structures confirms the conclusions drawn on the basis of the fluorescence spectra of the photoproducts, that the reaction of methoxyl radicals with the chromophore occurs quickly after the process of photocatalytic splitting of methanol and hydrogenation of the photocatalyst molecule.

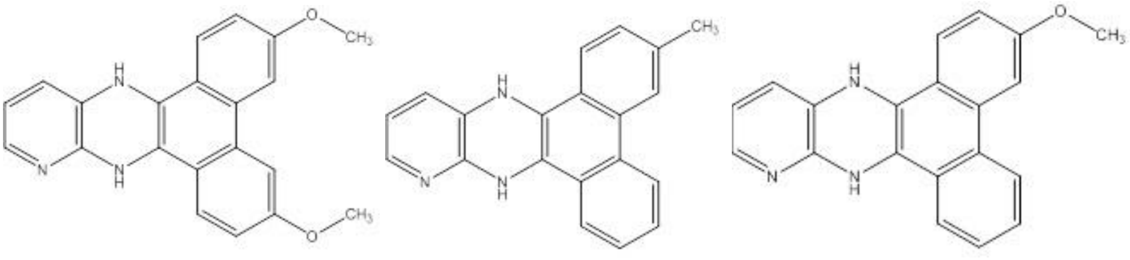

Figure 32. The most abundant in MS spectrum photoproducts of PQPhen. Positions of the attached groups in molecular structure of chromophore are ambiguous.

Also among the PQ2Py photoproducts are methoxylated or methylated structures of the doubly hydrogenated chromophore (Figure 33). However, for this photocatalyst, the mass spectra of the photoproducts include structures with masses lower than the mass of the substrate. Figure 33 shows one such structure. Its occurrence proves the decomposition of the chromophore during the photocatalytic process of methanol splitting. Decomposition may occur when methanol cleavage occurs at the pyrazine ring and the resulting methoxyl radical is located near the single bond between the pyridine ring and the pyrazine ring. Then the attack of the radical on a nearby carbon atom can "cut off" the pyridine ring. This decomposition of the chromophore causes the irreversibility of the PQ2Py hydrogenation process, which is manifested by irreversible changes in the absorption spectrum of the photocatalyst solution shown in Figure 29.

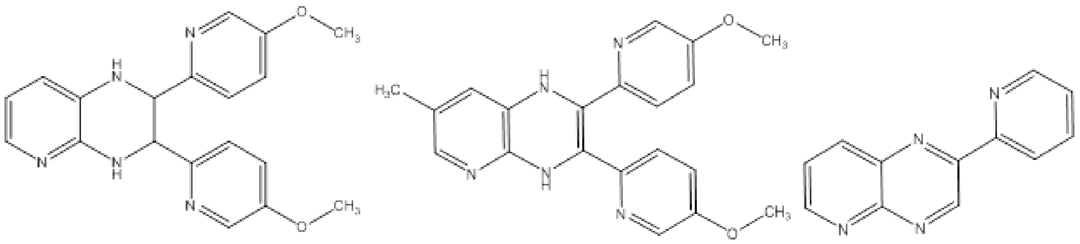

Figure 33. Examples of PQ2Py photoproducts appearing in the mass spectrum. The positions of the groups in the molecular structure are only suggestions.

The mass spectrum of the irradiated Q2Py solution, for which theory predicts barrier-free PCET, consists mainly of photoproducts with a mass less than the starting chromophore. Among them, there is a structure with only one pyridine ring, as was observed for PQ2Py, while most of the photoproducts are unidentified structures with the degree of unsaturation (double bond equivalent, DBE) reduced to 4.5 from 14.5 characterizing the starting chromophore. This indicates the presence of alkyl groups arising from the opening of aromatic rings attacked by radicals generated in the photocatalytic process.

Summarizing the results of all tests of PQPhem, PQ2Py and Q2Py molecules, it can be concluded that the most durable photoactive chromophore is PQPhen, which has a compact molecular structure, and the least durable is Q2Py, in which the PCET process in the gas phase is exothermic and the structure is branched with single bonds between the groups of the molecule.

Individual contributions from authors:

Olaf Morawski (75%) – defining the scope of experimental work, coordinating and conducting research outside the IF PAN, measuring optical spectra and fluorescence kinetics, preparing the results, writing the text of the article

Paweł Gawryś (10%) – synthesis of molecular material (PQPhem, PQ2Py and Q2Py), cyclic voltammetry measurements.

Andrzej L. Sobolewski (15%) – theoretical calculations, tables and figures with theoretical results, editing the text of the article

NMR and HRMS spectra measurements were performed as a paid service provided with the participation and supervision of OM at the Faculty of Chemistry of the University of Warsaw (NMR) and at the Institute of Organic Chemistry of the Polish Academy of Sciences in Warsaw (HRMS).

4.2 Another scientific achievement

4.2.1 Title of the another scientific achievement

Relationship between an increase of internal conversion efficiency and intramolecular charge transfer in some of polar organic molecules

4.2.2 Abstract

In the course of research on organic molecules with electro-donor and electro-acceptor functional groups, it was observed that the phenomenon of intramolecular electric charge transfer (ICT) is accompanied by a significant increase in the internal conversion rate constant. Combining the results of experimental research with the results of theoretical exploration of polar molecular structures makes it possible to explain the interdependence between both processes and indicate the change in the geometry of the excited state as the cause of this relationship.

4.2.3 Publications on which the another scientific achievement is based

[IOP1] K. A. Zachariasse, M. Grobys, T. von der Haar, A. Hebecker, Y.V. Il'ichev, O. Morawski, I. Rückert, W. Kühnle
J. Photochem. Photobiol. A, **1997**, *105* (2-3), pp. 373-383
Photoinduced intramolecular charge transfer and internal conversion in molecules with a small energy gap between S_1 and S_2. Dynamics and structure

[IOP2] I. Rückert, A. Demeter, O. Morawski, W. Kühnle, E. Tauer, K.A. Zachariasse
J. Phys. Chem. A, **1999**, *103* (13), pp. 1958-1966
Internal conversion in 1-aminonaphthalenes.: Influence of amino twist angle

[IOP3] O. Morawski, A. L. Sobolewski, B. Kozankiewicz, L. Sznitko and A. Miniewicz
Phys. Chem. Chem. Phys., **2014** , *16*, pp. 26887-26892
On the origin of fluorescence emission in optically non-linear DCNP crystals

[IOP4] O. Morawski, B. Kozankiewicz, A. L. Sobolewski and A. Miniewicz
ChemPhysChem, **2015**, *16* (16), pp. 3500 – 3510
Environment-sensitive Behavior of DCNP in Solvents with Different Viscosity, Polarity and Proticity

[IOP5] O.W. Morawski, L. Kielesinski, D.T. Gryko, and A.L. Sobolewski
Chem. Eur. J., **2020**, *26* (32), pp. 7281-7291
Highly Polarized Coumarin Derivatives Revisited: Solvent-Controlled Competition Between Proton-Coupled Electron Transfer and Twisted Intramolecular Charge Transfer

4.2.4 Description of the scientific achievement

4.2.4.1 Introduction

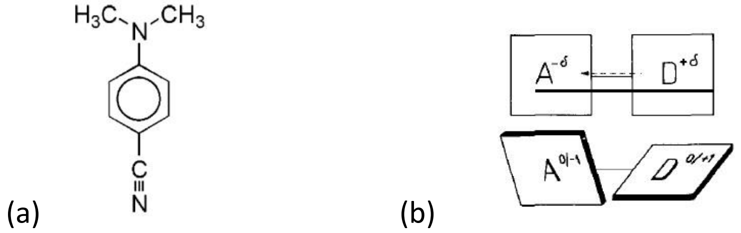

Figure 34. Molecular structure of DMABN (a) and structures proposed for excited states: local (LE) and twisted (TICT) (b).

Lippert's discovery of the dual fluorescence of dimethyl-amino-benzonitrile (DMABN, Figure 34) [1, 2] aroused great interest in this molecule and led to numerous works on it. Initially. the unusual phenomenon was interpreted as the result of the inversion of states of different polarity (Lippert) or the formation of excimers, exciplexes or proton transfer. These first proposals, however, were not experimentally verified and only Grabowski's concept of the existence of two excited electronic states with different geometry and polarity - a flat locally excited (LE) and a twisted, highly polar state with charge transfer (TICT - Twisted Intramolecular Charge Transfer) [3] – turned out to be a persistent and widely accepted explanation for DMABN's anomalous fluorescence violating Kasha's rule. Although the very concept of the existence of two different excited states was accepted, twist of the functional group (electron donor or acceptor) was questioned and several alternative explanations were proposed: the pseudo Jahn-Teller effect and donor re-hybridization (PJT) [4], acceptor re-hybridization (RICT) [5] and flat ICT (PICT) [6]. Although these ideas were also negatively verified over time, the very existence of controversy led to the creation of numerous and detailed experimental works not only on DMABN and its derivatives, but also on many other polar molecules in which rotation and, at the same time, intramolecular charge transfer, ICT, may occur. These studies have shown that usually the fluorescence quantum yield of ICT molecules is low and sometimes very low. However, non-radiative processes other than ICT were not the subject of interest and were mostly ignored in research and no general conclusion nor relationship between these processes was established.

References
[1] E. Lippert, W. Luder and H. Boos, in: Advances in molecular spectroscopy, ed. Mangini, Pergamon Press, Oxford, (**1962**) p. 443.
[2] E. Lippert, W. Liuder, F. Moll, W. Nagele, H. Boss, H. Prigge and I. Seibofd-Blankenstein, *Angew. Chem.*, 73 (**1961**) 695.
[3] K. Rotkiewicz, K.-H. Grellmann and Z. R. Grabowski, *Chem. Phys. Lett.*, 19 (**1973**) 315; erratum 21 (**1973**) 212.
[4] K.A. Zachariasse, T. von der Haar, A. Hebecker, U. Leinhos, W. Kuhnle, *Pure Appl. Chem.* 65 (**1993**) 1745.
[5] A.L. Sobolewski, W. Domcke, *Chem. Phys. Lett.* 250 (**1996**) 428.
[6] K.A. Zachariasse, M. Grobys, T. von der Haar, A. Hebecker, Yu. V. Il'ichev, O. Morawski, I. Ruckert, W. Kuhnle, *J. Photochem. Photobiol A*, 105 (**1997**) 373.

4.2.4.2 Studies on radiationless processes in molecules with intramolecular chargé transfer - discussion of publications IOP1 – IOP5

Below are short presentations of works that constitute another scientific achievement. The descriptions of the results do not contain literature references, as they are included in the content of the articles discussed.

4.2.4.2.1 Publication IOP1 –influence of the ^1L_a and ^1L_b states proximity on ICT process and dual fluorescence of some aminobenzonitriles

<u>Achievement:</u> noticing the efficient internal conversion process in aminonaphthalenes and linking the height of the energy barrier for the ICT process with the energy gap between the ^1L_a i ^1L_b states.

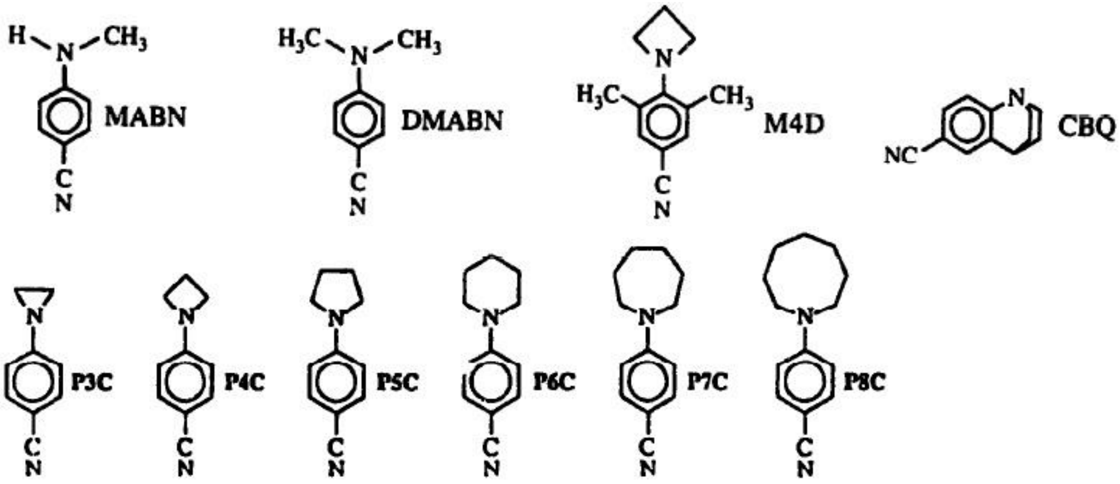

Figure 34. Molecular structures of aminobenzonitriles investigated optically in work IOP1.

Optical spectra of a series of aminobenzonitriles shown in Figure 34 allow to determine the relative position and energy gap between the ^1L_a and ^1L_b states. For MABN and DMABN molecules, the order of the lowest excited singlet states was determined to be $S_1(L_b)$ and $S_2(L_a)$, while for M4D and CBQ it was $S_1(L_a)$ and $S_2(L_b)$. Moreover, the occurrence of double fluorescence of DMABN and M4D molecules was associated with the small energy gap between these states, $\Delta E(S_1, S_2)$, and the lack of double fluorescence for MABN and CBQ - with the large energy gap $\Delta E(S_1, S_2)$ observed in these molecules. The large solvatochromism of the CBQ spectra was interpreted as emission from the CT state, $S_1(L_a, CT)$, and the smaller solvatochromism of the MABN spectra was interpreted as emission from the locally excited singlet ^1L_b, $S_1(L_b, LE)$. In this way, the possibility of the ICT process occurring in the molecule was determined - charge transfer in the excited state takes place if the lowest singlet has a CT character or is energetically close to the CT state located slightly above it.

Studies of a number of molecular structures P3C, ..., P8C of aminobenzonitriles emitting double (LE and CT) fluorescence have shown that the energy barrier of the ICT process decreases with the increase in the size of the heterocyclic ring and may also be related to the size of the energy gap $\Delta E(S_1, S_2)$.

Since in the series of aromatic hydrocarbons benzene - naphthalene - anthracene, the energy of ^1L_b state, which is the lowest in benzene, decreases slower than that of the ^1L_a state, so that in anthracene ^1L_a is the lowest excited singlet state, the study of several aminonaphthalenes as molecules offering closely located states with different character have been undertook. The molecules selected for this purpose: 1-(dimethylamino) naphthalene (1DMAN), 1-aminonaphthalene (1AN), 1-(methylamino)naphthalene (1MAN) and 2-(dimethylamino)naphthalene (2DMAN), offer a small energy gap $\Delta E(S_1, S_2)$ and the CT nature of one of the electronic states.

Optical studies of aminonaphthalenes in solvents of different polarities and in a wide temperature range did not confirm the occurrence of double fluorescence for any of the compounds. Effective internal conversion observed for all aminonaphthalenes, is particularly efficient for 1DMAN. This fact was associated with the proximity of the S_1 and S_2 states in this molecule. It was also noticed that the non-radiative relaxation rate constant decreases significantly in polar solvents, and the height of the non-radiative process barrier increases in them (Table 11). The observation was interpreted as the effect of increasing the energy gap $\Delta E(S_1, S_2)$ in polar solvents, however the exact mechanism was not established and continued research on this phenomenon was announced.

Table 11. Fluorescence quantum yield Φ, fluorescence decay time τ, radiative k_r, nonradiative k_{nr} rate constant and a barrier for nonradiative relaxation process E_{ic} for 1DMAN in solvents.

Solvent	Φ	τ [ns]	k_r [10^7 s^{-1}]	k_{nr} [10^7 s^{-1}]	E_{ic} [kJ/mol]
n-pentane	0.01	0.106	9.1	960	18.6
Diethyl eter	0.03	0.40	7.3	200	27.4
Acetonitrile	0.21	4.40	4.7	12	30.3

Individual contributions from authors:

K. A. Zachariasse - corresponding author, article editing, research initiator
M. Grobys – extension of experimental set-up construction
T. von der Haar – optical measurements for MABN, DMABN, M4D i CBQ
A. Hebecker – optical measurements for P3C, P4C, P5C
Y.V. Il'ichev – optical measurements for P6C, P7C, P8C
O. Morawski – optical measurements for aminonaphthalenes, noticing the effect of solvent’s dielectric constant on non-radiative relaxation rate constant
I. Rückert – elaboration of experimental results
W. Kühnle- synthesis of molecular material

4.2.4.2.2 Publication IOP2 – linking the non-radiative relaxation S1→S0 with the difference in the geometry of these states

Achievement: it was shown that the internal conversion rate constant in aminonaphthalenes is proportional to the rotation angle of the amino group

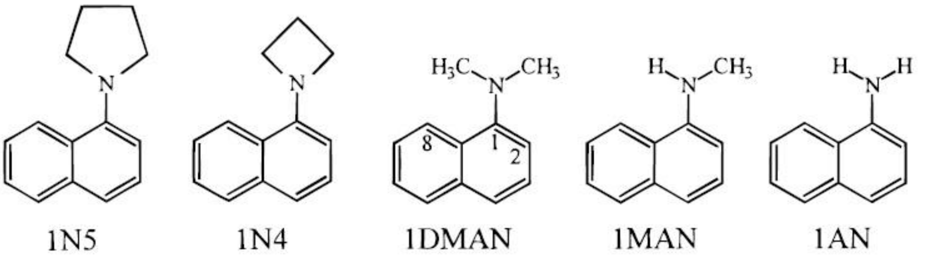

Figure 35. Molecular structures of aminonaphthalenes.

The study covered five molecular structures of aminonaphthalenes (Figure 35). *Ab initio* calculations showed that in the ground state the molecules have a similar dipole moment in the range of 1.1 - 1.8 D, which in the excited state increases to 7.1 - 8.1 D, as determined from the solvatochromism of spectra. None of the molecules exhibits double fluorescence and the (similar) fluorescence spectra are in a same spectral range with maximum intensity in the region of 25560 - 26520 cm^{-1} in n-hexane and 23160 - 23880 cm^{-1} in polar acetonitrile. The distinguishing feature of 1DMAN is the low fluorescence efficiency and short lifetime of the excited state observed in non-polar solvents (Table 12).

Table 12. Fluorescence decay time τ_F, quantum yields and rate constants, of radiatove transition Φ_F , k_r, intersystem crossing Φ_{isc} , k_{isc}, internal conversion Φ_{ic} , k_{ic} as well as a the height of internal conversion barrier, E_{ic}, for aminonaphthalenes in solvents.

Molecule	τ_F	Φ_F	Φ_{isc}	Φ_{ic}	k_r	k_{isc}	k_{ic}	k^0_{ic}	E_{ic}
25 °C	ns				10^7/s	10^7/s	10^7/s	10^{13}/s	kJ/mol
				n-heksane					
1N5	0.082	0.007	0.03	0.96	8.5	40	1200	1.1	17
1N4	1.73	0.14	0.13	0.73	8.4	8	40	1.5	26
1DMAN	0.120	0.01	0.02	0.97	8.3	15	830	1.2	18
1MAN	7.80	0.58	0.43	0.04	7.4	4	0.6	5.8	40
1AN	6.65	0.44	0.46	0.09	6.6	7	1.6	6.4	38
				Diethyl ether					
1N5	0.382	0.031			8.1				
1N4	5.96	0.45			7.6				
1DMAN	0.44	0.032	0.03	0.94	7.3	6	220	13	27
1MAN	11.7	0.82			7.0				
1AN	12.4	0.78			6.3				
				acetonitrile					
1N5	4.45	0.24	0.33	0.43	5.3	7	10	5.7	33
1N4	14.2	0.75	0.14	0.11	5.3	1.0	0.14	1.4	40
1DMAN	4.45	0.21	0.31	0.48	4.6	7	11	3.4	31
1MAN	17.7	0.92	0.09	0.0	5.2	0.5			
1AN	18.3	0.86	0.16	0.0	4.7	0.9			

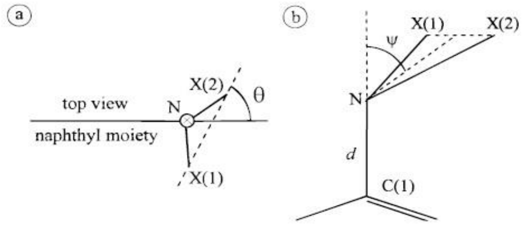

Figure 36. Definition of angles in structure of aminonaphthalenes: (a) twist of amino group θ and (b) the conical ψ.

Table 13. Amino group twit angle θ and conical ψ, the sum of angles of amino nitrogen bond with neighbouring carbons Σ(N) and length of N-C_1 bond obtained from Gaussian 94.

Parametr	**1N4**	**1DMAN**	**1MAN**	**1AN**
θ [°]	36	60	15	22
d [pm]	140.5	142.4	139.7	140.4
Σ(N) [°]	337	342	344	335
ψ [°]	38	41	38	47

As part of the search for the reason for the efficient internal conversion process in 1DMAN, calculations were made for the ground state of aminonaphthalenes, in particular its geometry, bond lengths and angle values: rotation of the amino group and conical angle (Figure 36 and Table 13, definition of the C_1 atom - Figure 35). It turned out that the logarithm of the internal conversion rate constant in n-hexane, k_{ic}, correlates well with the rotation angle of the amino group θ (Figure 37). Assuming that the twisted structure in the excited state changes to flat and there is a vibronic coupling between S_1 and energetically close S_2 state, which leads to the flattening of the S_1 potential energy surface, 1DMAN experiences the greatest change in the geometry of the excited state and the conical intersection of the potential surfaces of the S_1 and S_0 states occurs (Figure 38), which opens efficient relaxation to S_0 through the internal conversion channel. Thus, the relationship presented in Figure 37 illustrates the relationship between the degree of change in the geometry of the excited state and the rate of internal conversion $S_1 \rightarrow S_0$.

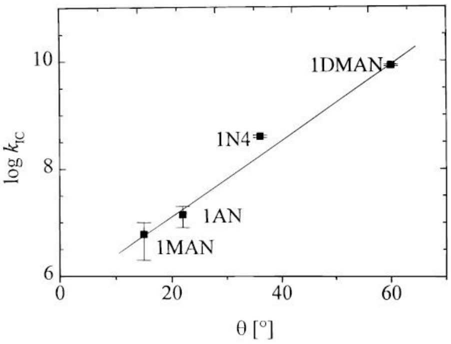

Figure 37. Logarithm of k_{ic} against angle θ in aminonaphthalenes.

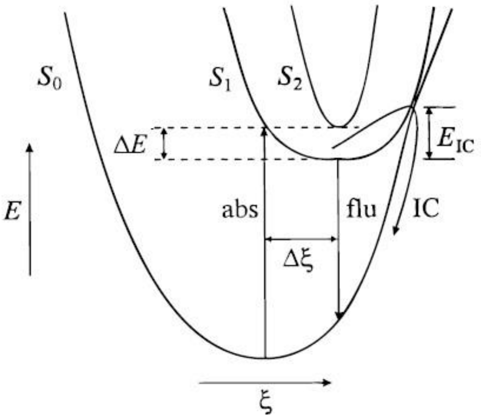

Figure 38. PES for S_0, S_1, S_2 states in 1DMAN as a function of coordinate containing angle θ. Conical intersection of S_0 with S_1 opens internal conversion.

Individual contributions from authors:
I. Rückert – experimental data elaboration and preparation of figures
A. Demeter – triplet formation yield determination (concept, apparatus)
O. Morawski –optical measurements and calculation of fluorescence decay times
W. Kühnle- synthesis of molecular material
E. Tauer – triplet formation yield determination (measurements)
K. A. Zachariasse - corresponding author, article editing

4.2.4.2.3 Publication IOP3 – DCNP – molecular rotor placed in crystal structure

<u>Achievement:</u> demonstrating that the emission properties of a molecule with internal rotation and the ICT process placed in a crystal depend on the location and type of traps

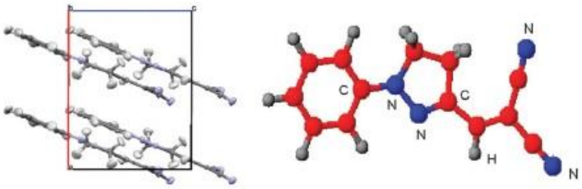

Figure 39. Crystal and molecular structure of DCNP.

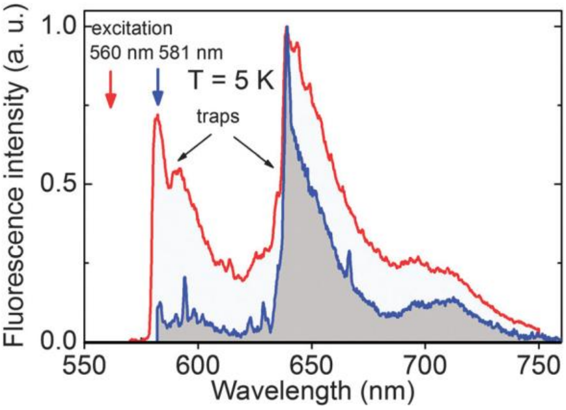

Figure 40. Emission spectra of DCNP crystal traps excited at λ=560 and 581nm.

3-(1,1-dicyanoethenyl)-1-phenyl-4,5-dihydro-1H-pyrazole (DCNP, Figure 39) is a highly polarized "push-pull" molecule - already in the ground state its dipole moment is 7.5 D and in the excited state it increases to 14.6 D. DCNP crystallizes in the monoclinic space group Cc without a center of symmetry (point group *m*) with a unit cell containing four molecules. The crystal is a ferroelectric structure, with high internal polarization $|P| = 0.116$ C m^{-2}, and the pyroelectric effect was observed for it. It shows effective two-photon absorption and also exhibits nonlinear optics properties, including second harmonic generation (*SHG*). Low-temperature (T = 5 K) studies of the DCNP single crystal showed that, in addition to emission from the excitonic band, there is fluorescence originating from several traps related to errors in the crystal structure (faults, vacancies) or to incorrect arrangement of molecules in the unit cell (anti-parallel instead of parallel arrangement of highly polar molecules in the unit cell). Trap states can be populated from the excitonic band or by selective optical excitation tuned to a specific trap (Figure 40). Temperature measurements have shown that thermal depopulation of shallow trap states leads to the filling of deeper traps. Detailed analysis of spectra and fluorescence decays shows differences in the emission properties of the traps and may be related to the fact that different traps may offer more or less free space for intramolecular torsion and rotation that the molecular structure of DCNP allows. As a result, the ICT process occurring upon optical excitation of DCNP may lead to changes in the geometry of the S_1 state depending on the volume of space offered by the trap in which the molecule is located. Facilitating the rotation reduces and limiting it increases the emission intensity of the molecule.

Individual contributions from authors:

Olaf Morawski (60%) – defining the research concept, measuring optical spectra and kinetics, writing the first version of the manuscript
Andrzej L. Sobolewski – theoretical calculation
Bolwsław Kozankiewicz – article editing
Lech Sznitko – measurement of Raman spectra
Andrzej Miniewicz – corresponding author, providing DCNP crystal for research

4.2.4.2.4 Publication IOP4 – influence of environment on fluorescence of molecular rotor

<u>Achievement:</u> demonstrating the influence of solvent polarity and proticity on the emission of the fluorescent molecular rotor - DCNP, and explaining the mechanism of this phenomenon

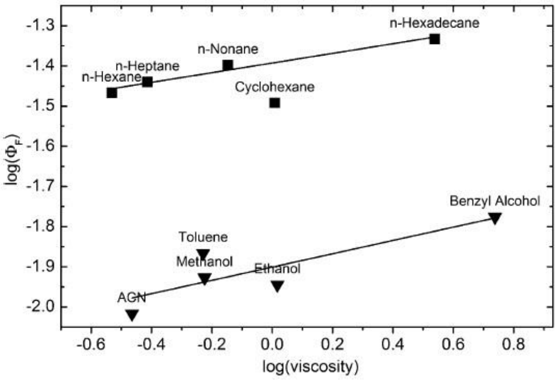

Figure 41. Log-log Φ_F dependence on η for DCNP in various solvents.

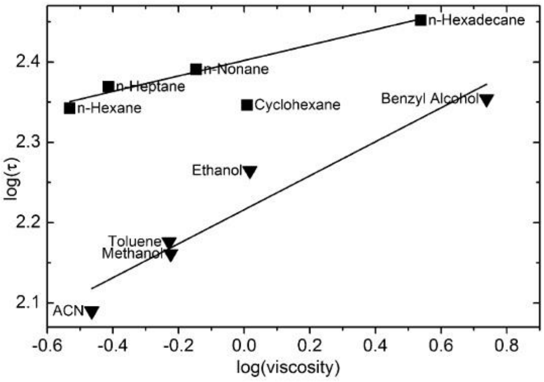

Figure 42. Log-log τ_F dependence on η for DCNP in various solvents

Fluorescent molecular rotors, a class of molecules with a structure that allows internal rotation and can create TICT emission due to intramolecular charge transfer, are of great interest because they can be used as molecular probes of the viscosity of the medium. The viscosity of the solvent ▯ slows down the intramolecular rotation affecting the emission properties of the molecule. Hence, the viscosity of the medium affects measurable quantities such as emission intensity or fluorescence quantum yield Φ_F. For small Φ_F, the relationship between viscosity η and efficiency Φ_F is expressed by the Förster-Hoffman formula: $\log(\Phi_F) = x \cdot \log(\eta) + C$, where x is an exponent whose value should be ⅔ and C is a constant. A similar formula holds for the fluorescence decay time, τ_F.

Figures 41 and 42 show in a log-log plot the Φ_F and τ_F values for the DCNP molecule in solvents of different viscosity, polarity and proticity. They show that this molecule behaves like a molecular rotor only in groups of solvents with a similar dielectric constant: nonpolar n-alkanes or polar alcohols and nitriles. The dielectric constant ε of the medium has a significant impact on the emission of DCNP and in polar solvents with $\varepsilon > 10$ both Φ_F and τ_F have significantly lower values than in n-alkanes for which $\varepsilon < 2$. In order to explain the phenomenon, quantum chemical calculations were performed for the DCNP molecule . The obtained isomer structures and state energies are presented in Figures 43 and 44.

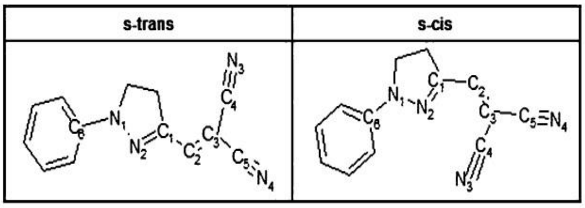

Figure 43. DCNP isomers structures and numbering of atoms.

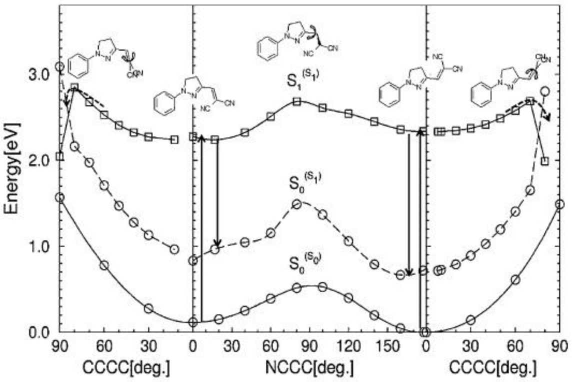

Figure 44. Energy of S_0 i S_1 states in function of dihedral angles $N_2C_1C_2C_3$ and $C_1C_2C_3C_4$.

In the ground state, the lowest energy structure is the *s-trans* isomer with dipole moment μ_g = 7.65 D. In the excited state S_1 it increases to μ_e = 14.59 D, which confirms the ICT in this molecule. The S_2 state is as much as 1.5 eV above S_1, so the two states do not mix. Rotation around the single C_1-C_2 bond changes the dihedral angle of $N_2C_1C_2C_3$ and transforms the *s-trans* form into the *s-cis* isomer, however, the high barrier of this rotation at S_0, 0.5 eV, prevents this process. In the S_1 state, the barrier height decreases to 0.35 eV and the potential surface flattens, allowing high-amplitude rotations. Similarly, the barrier to the rotation of the dicyano group around the C_2-C_3 double bond, which changes the $C_1C_2C_3C_4$ dihedral angle, decreases in S_1. This rotation leads to a conic intersection with the S_0 state, which opens an efficient channel for non-radiative relaxation to the ground state via the internal conversion path. The calculation results therefore confirm the possibility of large-amplitude rotation of DCNP fluorescence in the excited state, as in other fluorescent molecular rotors.

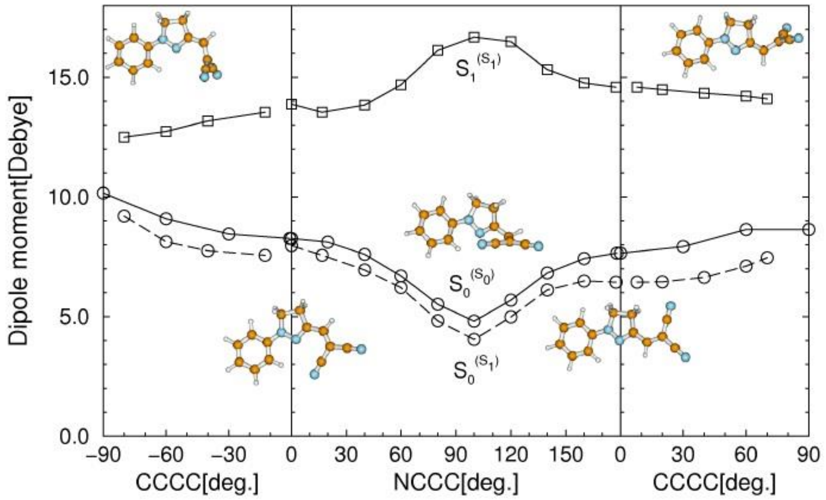

Figure 45.Dipole moment for S_0 (○) and S_1 (□) versus dihedral angles $N_2C_1C_2C_3$ and $C_1C_2C_3C_4$.

To explain the influence of the dielectric constant on the height of the barriers, value of the dipole moment μ in the S0 and S1 states were calculated along the reaction path (rotation angle) - Figure 45. It turned out that the polarization of the molecule increases with the rotation around the C1C2 bond from μ = 14.59 D for the dihedral angle N2C1C2C3 180° to μ=16.7 D at 90°. The increase in μ of the chromophore increases the energy of interaction with a polar or polarizable solvent and consequently lowers the energy of the electronic state. In fluorescence spectra, this manifests itself as solvatochromism - a shift in emission to lower energy, in the discussed case - as a lowering of the height of the rotation barrier. The barrier lowering can be estimated by treating the chromophore as a point electric dipole μ placed in a dielectric with constant ε. The presence of a dipole induces in the dielectric a reaction field $R = 2\mu /(4\pi\varepsilon_0 hca^3)\ f(\varepsilon)$, where a is the radius of the molecule and $f(\varepsilon)$ is a function of the dielectric polarizability of the solvent. The interaction energy $E = -\ \mu\cdot R = -(\mu^2/(2\pi\varepsilon_0 hca^3))f(\varepsilon)$. Assuming from DCNP quantum chemistry calculations, the Onsager cavity radius at a = 0.59 nm, the barrier height in polar methanol (ε = 32.66) drops from 0.35 to 0.16 eV, while in nonpolar n-nonane (ε = 2.0) to 0.27 eV. Therefore, in polar solvents, the rotation amplitude is larger and non-radiative transitions are more efficient. Hence, the emission intensity is lower and its decay time is shorter than in non-polar solutions. In both cases, however, the viscosity of the medium is important, as shown in Figures 41 and 42.

In several solvents (acetonitrile, methanol and ethanol), bi-exponential decays of DCNP fluorescence were observed, in all other solvents the decays were mono-exponential. The presence of a second, long-lived component in the three solutions was associated with the proticity of these polar solvents. Their proticity expressed by the parameter α determining the acidity of the hydrogen donor is 0.19, 0.83, 0.93, respectively. For other solvents used, α is equal to zero. The share of the long-lived component in the biexponential fluorescence decay measured by the ratio of both amplitudes increases proportionally to α as shown in Figure 46. Therefore, the occurrence of the long-lived component of the DCNP fluorescence decay has been associated with the formation of hydrogen-bonded complexes between the chromophore and the solvent molecule.

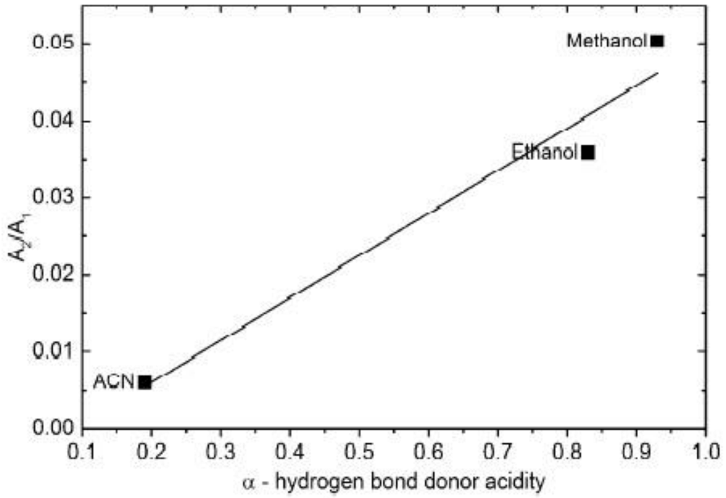

Figure 46. Ratio of long (A_2) to short component amplitude (A_1) of fluorescence decay in protic solvents in function of parameter α.

In addition to examining the influence of viscosity, polarity and proticity of the solvent on the emission of DCNP at room temperature, tests were performed in 5 - 300 K temperature range were undertaken for selected solutions. The research results showed that at low temperatures the most important factor influencing the intensity and duration of fluorescence is the viscosity of the medium.

Thus, it was shown that DCNP exhibits the features of a fluorescent molecular rotor, while also being a "sensor" of the proticity and polarity of the environment.

Individual contributions from authors:

O. Morawski – defining the experimental research scope, measurements of optical spectra and kinetics of fluorescence, elaboration of results, writing publication, corresponding author
B. Kozankiewicz – article editing
A. L. Sobolewski – theoretical calculation, tables and figures with theoretical results
A. Miniewicz – providing DCNP for research, article editing

4.2.4.2.5 Publication IOP5 – competition between two radiationless processes: TICT and PCET

Achievement: in the chromophore, in which the electron transfer leads to two different processes related to the change in the geometry of the excited state - TICT and PCET, the factor controlling their competition was identified and the adequacy of the theoretical models proposed for their description was checked.

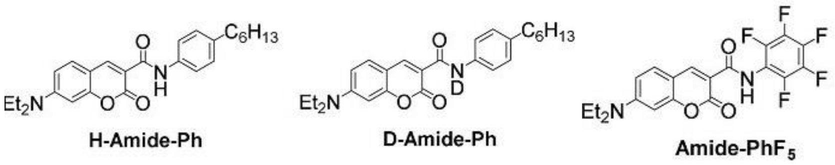

Figure 47. Molecular structure of the compounds.

In order to study proton transfer (PT), four 7-(diethylamino)-coumarin derivatives were synthesized, three with an amide bridge and one with an ester bridge, serving as a model molecule in which PT does not occur (Figure 47). Furthermore, in Amide-PhF$_5$, an electro-acceptor group of PhF$_5$ was placed to modify the energy conditions for PT, and in D-Amide-Ph, the labile hydrogen of the amide bridge was replaced with deuterium to capture differences in the expected PT.

Theoretical exploration showed that in all structures, electron transfer occurs during optical excitation, as a result of which the dipole moment increases significantly (Figure 48). In H-Amide-Ph, the theory indicates a barrier-free PT to the low-energy state and no emission, in the remaining molecules - occupancy of the locally excited state. In the polar medium, TICT is predicted for all structures (Figure 49).

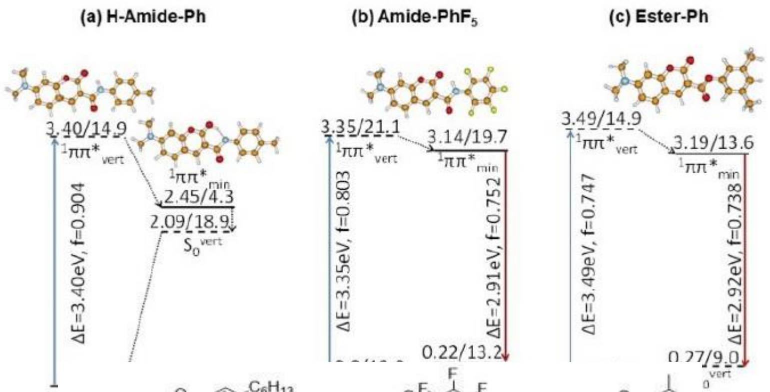

Figure 48. Energy (eV) / dipole moment (D) and energy of optical transitions (eV) with oscillator strengths (solid arrows) as well as radiationless relaxation (dashed arrows).

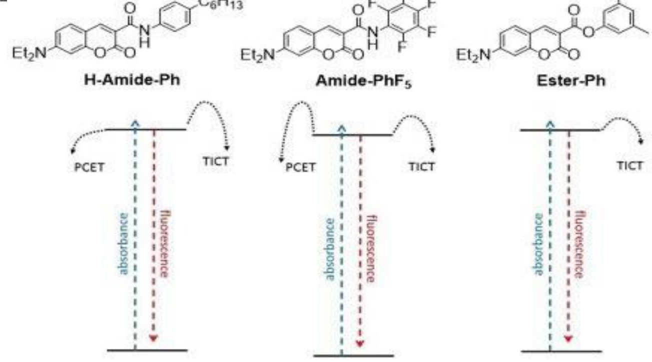

Figure 49. Simplified schema of photo- physical processes: Twisted Intra-molecular Charge Transter (TICT) and Proton-Coupled Electron Transfer (PCET).

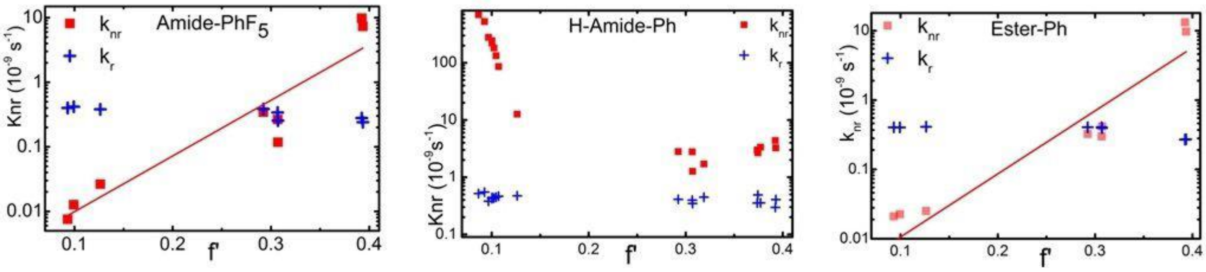

Figure 50. Rate constant of radiative (blue crosses) and radiationless (red squares) transitions of molecules in solvents as function of modified Lippert-Mataga polarity parameter f'.

All molecules in all solvents show fluorescence (not shown). No double fluorescence is observed and the fluorescence decay is always mono-exponential (not shown). The fluorescence quantum yield of Amide-PhF$_5$ and Ester-Ph is highest in nonpolar *n*-alkanes and decreases with solvent polarity. The lifetime changes similarly - it is longest in *n*-alkanes and shortened in polar solvents, indicating the intensification of the non-radiative process in the latter. Indeed, for these molecules, the radiative transition rate constant k_r does not depend on the polarity, while the non-radiative transition rate constant, k_{nr}, increases in proportion to the polarity of the medium (Figure 50). It is interpreted as an induced by the polarity of the solvent process of population non-emission TICT state.

The dependence of H-Amide-Ph emission on the polarity of the medium is very different - the lowest fluorescence quantum yield is observed in n-pentane and increases with the length of the *n*-alkane chain to reach a maximum in solvents with ε of the order of 10 - 20, and to decrease in the most polar ones. The fluorescence decay time changes analogously - it is the shortest in *n*-pentane, then it lengthens as ε increases and shortens for ε > 20. In H-Amide-Ph, the rate constant k_r also does not depend on the solvent, while k_{nr} changes the most and is the highest in nonpolar and non-polarizable medium (Figure 50). For D-Amide-Ph, similar changes are observed, but the deuterated form has a higher Φ_F and a longer τ_F, proving that proton/deuterium transfer occurs in the excited state of H-Amide-Ph and D-Amide-Ph molecules. The increase in k_{nr} in highly polar solvents indicates that TICT is also formed in this molecule, so two competing processes are active in it: TICT and PCET. Since the greatest changes in k_{nr} (k_{PCET}) occur in *n*-alkanes whose parameters, such as the dielectric constant or refractive index, change only slightly, H-Amide-Ph provides an opportunity to test theoretical models describing the PCET phenomenon and the parameters assumed in them. This is interesting because usually PCET and electron transfer in chromophores are examined in only one solvent and the functional groups of the chromophore are changed.

Rate constant of PCET process between initial μ and final vibronic state v is given as an extension of Marcus formula for electron transfer:

$$k_{PCET}(R) = \sum_{\mu,\vartheta} \frac{P_\mu}{\hbar} \left|V^{el} S_{\mu\vartheta}\right|^2 \sqrt{\frac{\pi}{\lambda k_B T}} \exp\left(-\frac{\left(\Delta G^0_{\mu\vartheta} + \lambda\right)^2}{4\lambda k_B T}\right) \tag{1}$$

where P_μ denotes Boltzman's population of substrate states, V^{el} electronic coupling, $S_{\mu v}$ integral of overlap for vibronic states of substrate and product, $\Delta G^0_{\mu v}$ is free energy for (μ, v) states and λ the total energy of reorganization. T and k_B have the ordinary meaning of absolute temperature and Boltzman constant. The free energy can be calculated with Weller approximation as:

$$\Delta G^0 = E^0(A^{\cdot +} A) - E^0(DD^{\cdot -}) - E_{0-0} - \frac{e^2}{4\pi \varepsilon_0 \varepsilon R_{AD}} \qquad (2)$$

where $E^0(A^{\bullet +}A)$ and $E^0(DD^{\bullet -})$ are reduction potentials of acceptor and donor groups, R_{AD} is chargé transfer distance and $E_{0\text{-}0}$ approximates difference between free Energy of initial and final states (usually excited LE and ground GS). Electrochemical potential depends on solvent and fo one electron oxidation and reduction in solvents *i* and *j* having dielectric constant ε_i and ε_j changes according to the expression:

$$E_i = E_j + \frac{e^2}{8\pi \varepsilon_0 FR}\left(\frac{1}{\varepsilon_i} - \frac{1}{\varepsilon_j}\right) \qquad (3)$$

where F is a Faraday constant and R a radii of Born cavity. Total Energy of reorganization λ is asum of inner sphere (chromophore) energy λ_i and outer sphere (solvent) energy λ_s, given by:

$$\lambda_s = \frac{e^2}{8\pi \varepsilon_0}\left(\frac{1}{n^2} - \frac{1}{\varepsilon}\right)\left(\frac{1}{R_A} + \frac{1}{R_D} - \frac{2}{R_{AD}}\right) \qquad (4)$$

where R_A and R_B are Born cavity radii of acceptor and donor, R_{AD} – a distance between them. In formulas (2) – (4) expressions like $1/\varepsilon$ and $1/n^2$ describe polarization of dielectric induced by a charge residing in Born cavity. They are clearly different from expression for polarization of dielectric induced by a point dipole residing in Onsager cavity. Moreover, yet another formulas for dielectric response are postulated for assumptions weaker than those of Born (details in publication IOP5). We used our experimental results for k_{PCET} and k_{TICT} in H-Amide-Ph to test different models of dielectric medium. It turned out, that classical and most often applied in literature expressions (2) – (4) correctly describe the trend of k_{PCET} in solvents as well as other values obtained from spectroscopy: energy of S_1 state and Stokes shift (details in publication IOP5).

Individual contributions from authors:

O.W. Morawski – scope of experimental tasks, measurements of spectra and fluorescence kinetic, data elaboration, writing the manuscript

Ł. Kielesiński – synthesis of molecular material, measurements of optical spectra

D.T. Gryko – article editing and writing

Andrzej L. Sobolewski – theoretical calculation, tables and figures with theoretical results

Awards

The article was featured with „Hot paper" label.

5. Presentation of significant scientific or artistic activity carried out at more than one university, scientific or cultural institution, especially at foreign institutions

5.1 Collaboration with Institute of Organic Chemistry PAS in Warsaw

5.1.1 Collaboration with prof. Daniel Gryko group

(A)
As part of the project "Organic ferroelectrics based on highly polarized coumarin systems", Łukasz Kielesiński from IOCh defended his thesis in 2020 entitled "Synthesis and optical properties of amido-coumarym" and obtained a PhD in physical sciences. The advisor was Prof. Daniel Tomasz Gryko, the supporting advisor was Dr. Olaf Morawski.

The doctoral thesis included four publications:

1. Ł. Kielesiński, O. Morawski, Ł. Dobrzycki, A. L. Sobolewski, D. T. Gryko, "The coumarin-dimer spring – the struggle between charge transfer and steric interactions" *Chem. Eur. J.*, **2017**, 23, 9174-9184. IF=5.160
2. Ł. Kielesiński, D. T. Gryko, A. L. Sobolewski, O. W. Morawski, "Effect of conformational flexibility on photophysics of bis-coumarins" *Phys. Chem. Chem. Phys.*, **2018**, 20, 14491-14503. IF=3.567
3. Ł. Kielesiński, Olaf W. Morawski, Andrzej L. Soboleski, Daniel T. Gryko, "The synthesis and photophysical properties of tris-coumarins" *Phys. Chem. Chem. Phys.*, **2019**, 21, 8314-8325. IF=3.567
4. Ł. Kielesinski, D. T. Gryko, A. L. Sobolewski, O. Morawski, "The interplay between solvation and stacking of aromatic rings governs bright and dark sites of benzo[g]coumarins" *Chem Eur. J.*, **2019**, 25, 15305-15314. IF=5.160

Moreover, in the framework of the mentioned program yet another paper was published:

5. O. W. Morawski, Ł. Kielesinski, D. T. Gryko, A. L. Sobolewski, "Highly polarized coumarin derivatives revisited: solvent-controlled competition between proton coupled electron transfer and twisted intermolecular electron transfer" *Chem Eur. J.*, **2020**, 26, 7281 –7291. IF=5.160

(B)
As part of the research on the emission properties of new and unusual coumarin derivatives, the following was published:
1. Ł. Kielesiński, I. Deperasińska, O. Morawski, K. V. Vygranenko, E. T. Ouellette, D. T. Gryko, "Polarized, V-Shaped, and Conjoined Biscoumarins: From Lack of Dipole Moment Alignment to High Brightness" *J. Org. Chem.* **2022**, 87, 5961–5975. IF= 3.6
2. L. Kielesinski, O. Morawski, C. A. Barboza, D.T.Gryko, "Polarized Helical Coumarins: [1,5] Sigmatropic Rearrangement and Excited-State Intramolecular Proton Transfer" *J. Org. Chem.* **2021**, 86, 6148–6159. IF= 3.6

5.1.2 Collaboration with Marek Grzybowski

As part of the cooperation, I undertook optical spectroscopy research on small organic molecules exhibiting chirality and infrared-active dyes. As a result, two joint works were created:

1. Marek Grzybowski, Olaf Morawski, Krzysztof Nowak, Paula Garbacz, "Fluorene analogues of xanthenes – low molecular weight near-infrared dyes", *Chem. Commun.*, **2022**, 58, 5455–5458. IF=4.9
2. Krzysztof Nowak, Olaf Morawski, Francesco Zinna, Gennaro Pescitelli, Lorenzo Di Bari, Marcin Górecki, Marek Grzybowski, "Strong chiroptical effects in the absorption and emission of macrocycles based on the 2,5-diaminoterephthalate minimal fluorophore", *Chem. Eur. J.*, **2023**, 29, e202300932. IF=5.160

A third publication on phosphorescence emitted at room temperature by pyrene derivatives is in preparation.

5.2 Collaboration with Faculty of Chemistry, Technical University of Wrocław

As part of cooperation with the team of Prof. Andrzej Miniewicz from the Wrocław University of Science and Technology, I conducted research on the polar molecular structure of DCNP. As a result, the following articles were published:

1. O. Morawski, A. L. Sobolewski, B. Kozankiewicz, L. Sznitkob and A. Miniewicz, "On the origin of fluorescence emission in optically non-linear DCNP crystals", Phys. Chem. Chem. Phys. **2014**, 16, 26887 -26892. IF=3.567

2. K. Cyprych, L. Sznitko, O. Morawski, A. Miniewicz, I. Rau, J Mysliwiec, "Spontaneous crystalization and aggregation of DCNP pyrazoline-based organic dye as a way to tailor random lasers", *J. Phys. D*, **2015**, 48, 195101. IF=3.409

3. O. Morawski, B. Kozankiewicz, A. L. Sobolewski, A. Miniewicz, "The environment-sensitive behavior of DCNP in solvents with different viscosity and polarity", *ChemPhysChem* **2015**, 16, 3500 – 3510. IF=3.52

6. Presentation of significant scientific or artistic activity carried out at more than one university, scientific or cultural institution, especially at foreign institutions

6.1 *Classes with students*

Computer science exercises (numerical methods) with students of the School of Exact Sciences at the Polish Academy of Sciences (1993).

6.2 *Summer internships for students*

Organization of monthly summer internships in the Molecular Photophysics Team (ON2.1 Team) and supervision of internships for physics students:

August 2015 - Michał Doliński, Faculty of Physics, Technical University of Warsaw
July 2016 - Damian Włodzyński, Faculty of Physics, University of Warsaw
August 2017 - Michał Piotr Matycz, Faculty of Physics, University of Warsaw
September 2017 - Mateusz Surma, Faculty of Physics, Technical University of Warsaw

6.3 *Doctoral student supervision*

In the years 2016 - 2020, Dr. Olaf Morawski, acting as an supporting supervisor of doctoral student Łukasz Kielesiński from the Institute of Organic Chemistry of the Polish Academy of Sciences in Warsaw, introduced him to the methods and optical spectroscopy equipment used in the ON2.1 IF PAN team and then cooperated with him by examining the properties of amido-coumarins. The result of this joint work is five publications.

In 2020, Łukasz Kielesiński defended his thesis entitled "Synthesis and optical properties of amido-coumarym" obtaining a Ph.D. in physical sciences. The promoter was Prof. Daniel Tomasz Gryko, the supporting supervisor was Dr. Olaf Morawski.

6.4 *Seminars*

Seminars outside Institute of Physics PAS
At the invitation of Prof. Jacek Waluk from the IPCh PAS I have presented two seminars:
2017 – *„The direct photocatalytic partial water oxidation - the new approach to water splitting”*
2023 – *„Photochemical Hydrogen Storage with Hexaazatrinaphthylene (HATN). Advantages and disadvantages.”*
Seminars at the Institute of Physics PAS (only last years)
2916 – “T*he new concept of water splitting”*
2023 – *„Photochemical Hydrogen Storage with Hexaazatrinaphthylene”*

6.5 *Experimental demonstrations in schools*

1. Show "Light as a wave. From the deflection (diffraction) of light to the study of the chemical composition of stars.” 18/05/2019, Mikołaj Kopernik Primary School, ul. Główna 10, 05-540 Ustanów.
2. Demonstration physics lesson (optics) „Molecules and light”, 12-IX-2019, Zespół Szkół im. Cecylii Plater-Zyberkówny, ul. Piękna 24/26 w Warszawie.

6.6 Support for econophysics section of Polish Physical Society (Sekcja PTF FENS)

1. Co-financing by HP Polska of the conference *„I Sympozjum z Ekono- i Socjofizyki”*, Warszawa 2004
2. Writing publication https://old.ptf.net.pl/fens/studia/ekonofizyka/olaf.morawski.pdf
3. Intership organization https://old.ptf.net.pl/fens/studia/ekonofizyka/hp.html

7. Other information – development of experimental apparatus and methods

After my PhD:

(A) I launched the first supersonic beam apparatus in Poland for optical research of organic molecules.

(B) I significantly facilitated the measurement of spectra on a phosphorimeter built around a helium cryostat based on a double photon counter card and a self-written *EasyScan* computer program, which, using the above-mentioned photon counter and controlling stepper motors, automated the registration of fluorescence and phosphorescence spectra, enabling their plotting in real time on the computer screen, and after the measurement is completed –processing and saveing them to the hard drive. Since the successful automation, all low-temperature spectra (range 5 – 300 K) are recorded and collected in the ON2.1 Team using the *EasyScan* program.

(C) I created software controlling a confocal microscope used to study single molecules in a wide range of temperatures (*Msw31* program). The program controls the movement of galvo scanners and controls the multiscaler card recording single photons emitted by molecules. All single-molecule papers published by ON2.1 Team employees use data recorded using the *Msw31* program.

(D) I built a test stand for photochemical processes that records in real time, with sub-second time resolution, changes in the fluorescence spectra of substrates and photo-products occurring during photo-irradiation of solutions. The stand has been computerized.

(E) I built a stand for recording photocurrents generated during exposure to solutions of photochemically active molecules, enabling measurements of low currents.

O. Morawski

…………………………………………………………